Geothermal, Oceanic, Wildfire, Meteorological and Anthropogenic Impacts on PM$_{2.5}$ Concentrations in the Fairbanks Metropolitan Area

Nicole Mölders[1,2], Gilberto Javier Fochesatto[1,2], Stanley Gene Edwin[1,3], Gerhard Kramm[4]

[1]University of Alaska Fairbanks, Department of Atmospheric Sciences, Fairbanks, USA
[2]University of Alaska Fairbanks, Geophysical Institute, Fairbanks, USA
[3]Council of Athabascan Tribal Governments, Fort Yukon, USA
[4]Engineering-Meteorology-Consulting, Fairbanks, USA
Email: cmoelders@alaska.edu

Abstract

The impacts of low and high-frequency variability from teleconnections between large scale atmospheric processes and local weather as well as emissions changes on concentrations of particulate matter of 2.5 μm or less in diameter ([PM$_{2.5}$]) were examined for the Fairbanks Metropolitan Area (FMA). October to March and May to August mean [PM$_{2.5}$] were 1.8 and 3.1 μg·m^{-3} higher for positive than negative annual mean Pacific Decadal Oscillation. Annual mean [PM$_{2.5}$] were 3.8 μg·m^{-3} lower for positive than negative Southern Oscillation Index. On 1999-2018 average, [PM$_{2.5}$] decreased 2.9 μg·m^{-3}·decade^{-1}. On average over October to March, decadal and inter-annual variability caused higher or similar differences in mean observed [PM$_{2.5}$] and its species than emission-control measures. The 2006 implementation of Tier 2 for new vehicles decreased observed sulfate concentrations the strongest (~4.95 μg·m^{-3}·decade^{-1}) of all occurred emissions changes. On average, observed [PM$_{2.5}$] showed elevated values at all sites when wind blew from directions of hot springs. The same was found for the sulfate, ammonium and non-metal components of PM$_{2.5}$. Observations showed that these geothermal waters contain sulfate, ammonia, boric acid and non-metals. Hot springs of such composition are known to emit hydrogen sulfide and ammonia that can serve as precursors for ammonium and sulfate aerosols.

Keywords

Concentrations, Emissions Impacts on $PM_{2.5}$ Concentrations, $PM_{2.5}$ Speciation, H_2S from Hot Springs

1. Introduction

Concentrations of particulate matter of 2.5 μm or less in aerodynamic diameter ($PM_{2.5}$) are of concern for air-quality regulations because of its adverse effects on human health at both long-term and short-term exposure [1] [2] [3] [4] [5]. In 2006 based on new medical insights, the US Environmental Protection Agency (EPA) tightened the 24-h National Ambient Air Quality Standard (NAAQS) for $PM_{2.5}$ from 65 μg/m³ to 35 μg/m³ to reduce health risks. The annual standard remained at 15 μg/m³. Under the new 24-h standard, daily mean [$PM_{2.5}$] less or equal 12 μg·m⁻³, and in the ranges of 12.1 - 35.4 μg·m⁻³, 35.5 - 55.4 μg·m⁻³, 55.5 - 150.4 μg·m⁻³, 150.5 - 250.4 μg·m⁻³ and greater or equal 250.5 μg·m⁻³ are considered good, moderate, unhealthy for sensitive groups, unhealthy, very unhealthy and hazardous, respectively [6]. Communities, for which the last three years of $PM_{2.5}$ monitoring prior to 2006 showed violation of the new 35 μg/m³ standard, were designated $PM_{2.5}$-nonattainment areas. They had to develop state implementation plans to get into and remain in compliance. These strategies were due no later than three years from the effective day of designation.

One of these communities was the Fairbanks metropolitan area (FMA), which encompasses Fairbanks, College, and the city of North Pole in Interior Alaska. In the FMA, $PM_{2.5}$ concentrations ([$PM_{2.5}$]) have frequently exceeded the 2006 24-h NAAQS in November to February since the onset of monitoring in 1999 [7]. Until 2006, [$PM_{2.5}$] higher than 35 μg·m⁻³, but lower than 65 μg·m⁻³ did fulfill the then NAAQS. Prior to 2006, exceedances occurred during various wildfire seasons.

Fairbanks (64.84N, 147.72W) had faced an air-quality issue caused by high concentrations of carbon monoxide (CO) at the beginning of this century [8]. The unfortunate combination of the city's location with respect to topography, the mean general circulation and its local climatological conditions were identified as the major causes [8]. Fairbanks is surrounded by the Yukon-Tanana uplands that build a three-sided bowl, which opens to the Tanana Flats toward the south to southwest (**Figure 1**). The low insolation levels at high latitudes yield a negative radiation flux balance and the formation of surface-based inversions (SBI) [9] [10]. The vicinity to the semi-permanent Canadian High supports calm wind accompanied by low to no-shear production of turbulent kinetic energy [9] and subsidence inversions [11].

Under inversion conditions, the stratification of the near-surface atmosphere becomes extremely stable. In winter, observations showed vertical temperature gradients of up to 30°C·100⁻¹ m; while [$PM_{2.5}$] were non-sensitive to the degree of stability, they were systematically highest under stable conditions [7]. Temperature inversions suppress vertical mixing and the exchange of polluted air
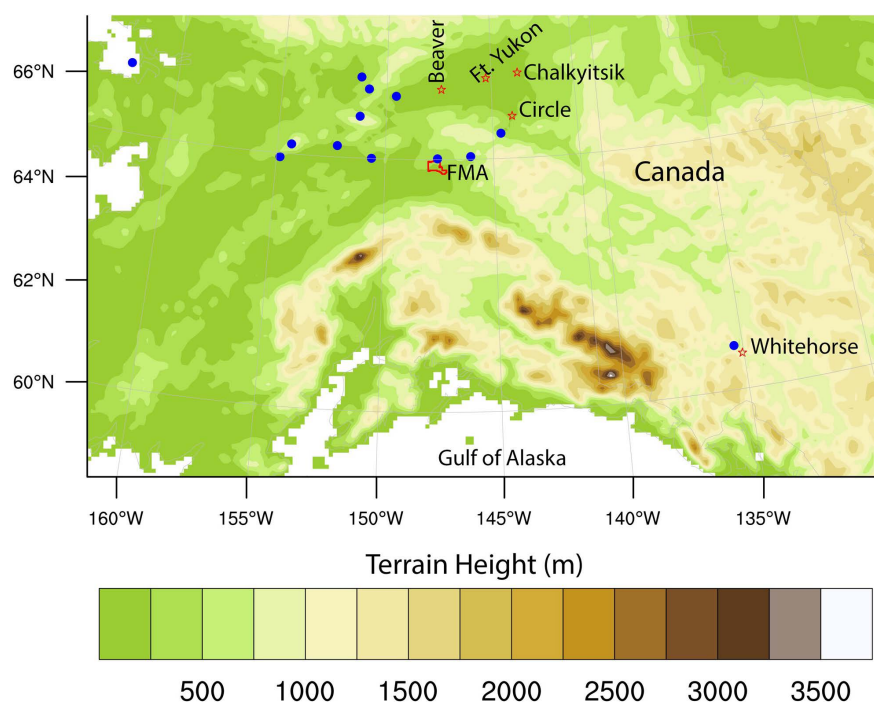
Figure 1. Location of the Fairbanks metropolitan area (FMA) nonattainment area (red polygon), the villages of Beaver, Chalkyitsik, Circle and Ft. Yukon in the Yukon Flats superimposed on the topography of Interior Alaska and South Alaska. Blue dots indicate locations of known hot springs.

with air aloft. Despite Fairbanks has no major industry [12], emissions of gaseous compounds like CO, sulfur dioxide (SO_2), and nitrogen dioxides (NO_2) and aerosols from traffic, power-generation and heating accumulate underneath these often multi-day inversions. Here chemical reactions, aerosol physical and chemical processes form secondary pollutants and aerosols.

Improved engine technology and the turn-over of the vehicle fleet as well as a mandatory biennial check of vehicle emissions eventually "solved" the CO air-quality issue [8]. The new technology led to more efficient combustion processes thereby reducing CO emissions. The more than 150 percent increase of the prices for gasoline and diesel fuel in the first decade of this century may have decreased fuel consumption by individual traffic, and may have contributed to reduced CO emissions as well.

In case of $PM_{2.5}$, such simple solution must not be expected even though solid fuel appliances like wood- and coal-fired stoves, and hydronic heaters have become more efficient. None of the potential direct (wood-stove change-out, introduction of natural gas), indirect (introduction of low sulfur fuel) and multiple emission-control measures (replacing wood with gas heating and use of low sulfur fuel) simulated for October 1, 2008 to March 31, 2009 with the Weather Research and Forecasting (WRF) model inline coupled with chemistry packages (WRF/Chem) [13] would provide design values below 35 $\mu g \cdot m^{-3}$ [14]; benefits for air quality would vary in persistence among measures [14]. Exchanging 2930

uncertified woodstoves and 90 outdoor wood boilers with EPA-certified wood-burning devices, for instance, would have reduced the 24-h average $[PM_{2.5}]$ by 0.6 $\mu g \cdot m^{-3}$ (6%), on average over the October to March 2008/09 cold season; this measure would have avoided only seven out of 55 simulated exceedance days [15]. Highest reductions on any exceedance day ranged from 1.7 to 2.8 $\mu g \cdot m^{-3}$; relative response factors were consistently low (~0.95) for all $PM_{2.5}$ species and months [15]. The 2008-design value of 44.7 $\mu g \cdot m^{-3}$ would be reduced to 42.3 $\mu g \cdot m^{-3}$ [14]. Sensitivity studies suggested that the benefits of a wood-burning device change-out program heavily relies on the accuracy of the estimates on how many devices exist that can be exchanged [15].

Substituting all wood by gas heating would reduce $PM_{2.5}$ emissions by ~11% yielding a design value of 38.9 $\mu g \cdot m^{-3}$. Burning low-sulfur fuel in oil-fired furnaces and facilities would reduce total SO_2 and $PM_{2.5}$ emissions by ~23% and 15%, respectively, and the design value to 42.8 $\mu g \cdot m^{-3}$ [14]. Concurrent replacement of wood-heating with gas heating and introduction of low–sulfur fuel would reduce SO_2 and $PM_{2.5}$ emissions by ~36 and 19%, respectively, and the design value to 39.3 $\mu g \cdot m^{-3}$. The benefits of using low-sulfur fuel depended the strongest on the meteorological regime. Unfortunately, the benefits of the multiple emissions-control measures generally fail to be the sum of the benefits of the respective single measures [14].

WRF/Chem simulations with and without consideration of point-source emissions revealed that 1) on days and at locations where $[PM_{2.5}]$ exceeded 35 $\mu g \cdot m^{-3}$, point-source emissions typically only contributed 4% to the 24-h average $[PM_{2.5}]$; and 2) point-source emissions induced only five additional exceedance days in the Fairbanks nonattainment area [16]. Highest concentrations occurred in the same locations in both simulations. Point-source emissions influenced $[PM_{2.5}]$ at breathing height strongest about 10 - 12 km in their downwind [16].

Various studies linked wildfire smoke, especially particulate matter at the micron- to sub-micron size, ozone (O_3) and volatile organic compounds (VOC) with increased risks of respiratory disease, cardiovascular diseases and mortality [1] [2] [17] [18] [19]. In the taiga region around the FMA, boreal wildfires are a natural component of the landscape evolution. Over the past decades, the annual wildfire activity and area burned have increased [20]. During the 2004- and 2005-wildfire seasons, for instance, Fairbanks 24-h average $[PM_{2.5}]$ was up to a factor of 20 and 11 higher than the current NAAQS. In both fire seasons, air quality became hazardous. Thus, from a health perspective, the $PM_{2.5}$ problem in the FMA may be more severe during the wildfire seasons than during extreme multi-day inversions in winter.

Obviously, besides local emissions, external factors like the general circulation, meteorology, geography and geological processes influence $[PM_{2.5}]$ in the FMA. The goal of our study was to determine the magnitude of these external (*i.e.* non-manageable) factors in comparison to observed $[PM_{2.5}]$ changes in response to well-known emissions changes.

2. Experimental Design

We hypothesized that in the FMA, the magnitude of $[PM_{2.5}]$ is due to a combination of the general circulation, synoptic and mesoscale features as well as weather-related natural and anthropogenic emissions, and if so, low-frequency variability and its impacts on local weather (and hence local emissions and $[PM_{2.5}]$) could pretend/dilute changes occurring in response to emissions changes in observed $[PM_{2.5}]$.

2.1. Data Sources and Processing

We downloaded public-available surface-meteorological, fuel, lysimeter and radiosonde data of Fairbanks, air-quality data of the FMA, fire [21] and anthropogenic emissions [12] data as well as data of the Pacific Decadal Oscillation (PDO), North Pacific (NP) and Southern Oscillation (SOI) Index. Data sources and times of availability are listed in Tables A1-A2 in Appendix A.

The PDO, NP and SOI indices describe different aspects of the general circulation known to influence weather in Alaska via large-scale teleconnections [22] [11]. Teleconnections are preferred modes of low-frequency (long time scale) variability. The NP is the monthly area-weighted sea-level pressure over 30N to 65N and 160E to 140W [23]. It measures inter-annual to decadal variations of the atmospheric circulation. The SOI is the normalized pressure difference between Tahiti and Darwin [24]. It gauges the strength of El Niño and La Niña events. The PDO refers to an irregularly recurring pattern of ocean-atmosphere variability over the mid-latitude central Pacific. It is defined by the monthly mean sea-surface temperature anomalies from the 1901-2000 climatology onto their first Eigen Orthogonal Function (EOF) vectors in the North Pacific north of 20N [25] [26]. To calculate the correlation of these indices with $PM_{2.5}$, monthly means of 24-h average $[PM_{2.5}]$ were determined.

Available air-quality data for the FMA encompass different species for various periods, at different temporal resolutions and locations (see Appendix A for details). Datasets considered in this study include CO, SO_2, NO_x, O_3, 1-in-3-days $PM_{2.5}$, daily mean $PM_{2.5}$ concentrations and 1-in-3-days speciation. Aerosol-speciation data considered sulfate (SO_4), nitrate (NO_3), ammonium (NH_4), organic carbon (OC), elemental carbon (EC), the following metals aluminum, calcium, chloride, copper, iron, lead, nickel, potassium, silicon, sodium, stadium, titanium, vanadium, tin, and non-metals bromine, and selenium. Speciation data at Pioneer Rd and North Pole are courtesy to the Fairbanks Air Quality Division. Beaver, Chalkyitsik, Circle and Ft. Yukon $[PM_{2.5}]$ data are courtesy to the Council of Athabaskan Tribal Government and the Tribes of Beaver, Chalkyitsik, Circle and Ft. Yukon.

2.2. Data Analysis

To test our hypothesis air quality had to be examined in a climatological sense. Therefore, we determined climatology of $PM_{2.5}$, its speciation, meteorological

and wildfire relevant conditions at the decadal, multi-year, annual, seasonal, monthly and daily scales. Following common practice (e.g. [27] [28]) we measured inter-annual variability by the temporal standard deviations.

To assess low frequency impacts we examined monthly means of [$PM_{2.5}$] for correlations with the NP, SOI and PDO. In our study, all correlations were examined for their significance at the 95% confidence level ($p < 0.05$) using paired two-tailed t-tests [29]. Following common practice [29], the number of data was considered in determining p for small samples.

Since [$PM_{2.5}$] can be high due to fires as well as anthropogenic emissions, we examined warm (May to August) and cold (October to March) seasonal means as well as monthly means of concentrations and meteorological features. In the following, May to August and October to March are called the warm and cold season, respectively.

At the $PM_{2.5}$ monitoring sites, some meteorological data (wind speed, pressure, minimum, maximum and mean hourly air and dew point temperatures) were recorded. However, an assessment of the synoptic (meso-α-scale) and meso-β-scale (temporal scales of 1 to 3 days) influences on [$PM_{2.5}$] requires a full suite of meteorological and—in the fire season—fire-relevant data. Therefore, we used the data from the Bureau of Land Management (BLM) Fairbanks site (64.83667N, 147.615W). In addition to 10-m wind speed and direction, 2-m air temperature, 2-m relative humidity, precipitation and pressure, this site also had long-term records on fire-relevant data like daily mean, maximum and minimum fuel temperatures and humidity as well as daily accumulated radiation at the surface. The latter is of interest for inversions caused by radiation deficit, and for photolysis that may initialize some summer aerosol formation paths. Also smoke may reduce solar radiation reaching the surface and photolysis rates.

Daily means and higher moments [29] calculated at various sites within the FMA were compared to capture meso-γ-scale (local, short-term) meteorological influences on [$PM_{2.5}$].

Empirical Orthogonal Functions (EOF) [29] [30] were determined for the time series of daily means of solar insolation, temperature, wind speed, relative humidity and $PM_{2.5}$ at various temporal scales. Fast Fourier Transformation (FFT) [29] [30] analysis on [$PM_{2.5}$] time series served to identify amplitudes, frequency and variances in individual cold seasons.

To examine whether [$PM_{2.5}$] changes due to low frequency variability could pretend success or failure of emission-control measures, we determined the magnitude of the following well-known emission changes using observed [$PM_{2.5}$] and its composition:

- In 2004, new passenger vehicles had to comply with the Tier 2-Motor Vehicle Emissions Standards and Gasoline Sulfur Control Requirements. They had to be 77% to 95% cleaner than those produced prior to 2004.
- Due to the drastic increase in fuel prices that peaked in 2007, many people added woodstoves to reduce heating costs [15].
- Since June 1, 2010, diesel fuel used in rural Alaska and on highways had to

meet the same 15 ppm (maximum) sulfur-content standard than that used in Alaska's cities. Inhabitants from rural communities north of Fairbanks frequently come into town for shopping. The FMA is also a traffic junction of six major highways.

- In June 2010, the Fairbanks North Star Borough (FNSB) started a wood-stove change-out program. Qualifying old wood-stove devices were replaced by more efficient EPA-certified ones to reduce the emissions of $PM_{2.5}$ and its precursor gases.

Finally, to assess potentially overlooked emission sources we turned to the literature and data from Alaska sites outside the FMA as available.

3. Results

3.1. Climatological Features

Fairbanks is the largest city in the Interior. No other conurbations exist in a radius of 417 km (Figure 1). In the FMA, daily totals of solar radiation reaching the top of the atmosphere (TOA) and Earth's surface are low between early November and end of February (Figure 2(a)). Solar radiation reaching the surface peaks earlier than at the TOA as humidity and cloudiness increases from March towards August. In the fire season (May-August), high particle loading due to fires may also reduce the solar radiation at the surface [22]. The huge amounts of water vapor released from evaporation and sublimation of soil water and ice due to fires burning on permafrost also may decrease solar radiation at the surface [31].

Usually, the snowfall season is September to May (Figure 2(b)). During this time the snow cover leads to high solar albedo. The solar irradiance absorbed by the snow and underlying soil is marginal. The fire season in the Interior usually starts in May, when the global radiation and near-surface air temperatures are already relatively high, but precipitation is still relatively low (Figure 2(a) and Figure 2(b)).

According to the 1981-2010 climate record at Fairbanks International Airport (134 m, 64.8039N, 147.8761W), daily mean temperatures below and above freezing occur from September through April and May through August, respectively (Figure 2(b)). Rarely temperatures are below −40˚C or above 28˚C. From early November to end of February, near-surface air temperatures are usually below −10˚C. The diurnal temperature range is about 9 K in November and 13 K in February [22]. Summers are cool and humid with the maximum of monthly precipitation in August. March is typically the driest months. September to April relative humidity varies between 40% and 90%. Wind speed is generally low through the year with June having the highest monthly average wind speed (6.35 m·s⁻¹).

The FMA's frequent SBI in winter are among the strongest anywhere [8] and persist much longer than in mid-latitudes [7]. Daytime and nighttime SBI occurred on about 82% of the days in December and January, and on about 68% of
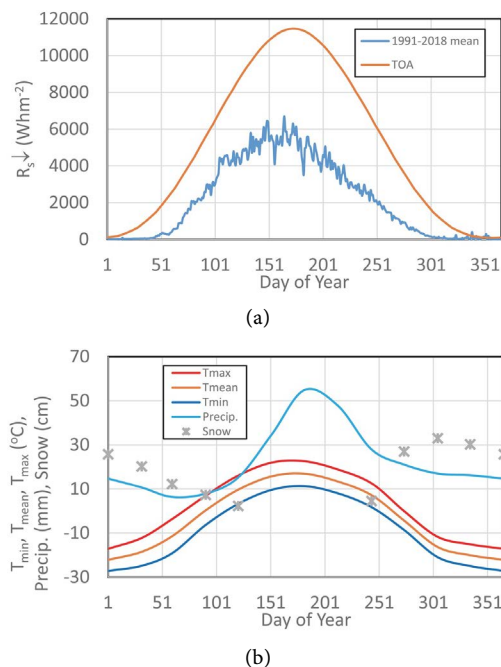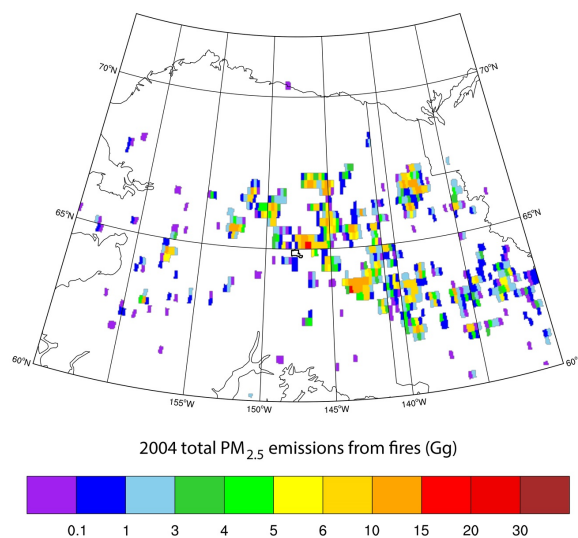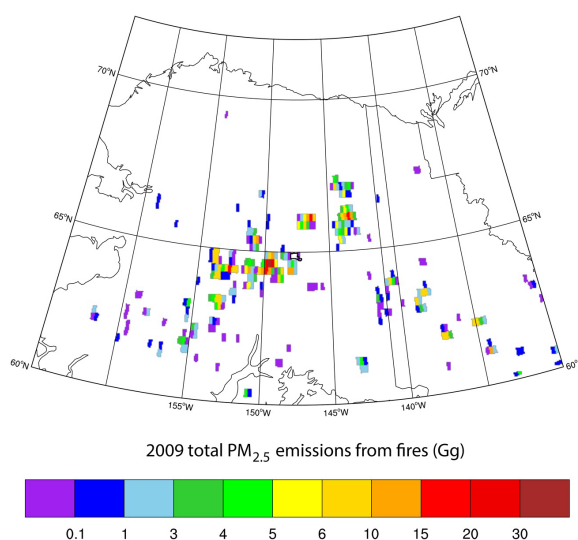
(a)

(b)

Figure 2. Long-term mean meteorological conditions in the FMA. (a) Annual cycle of daily total solar downward radiation ($R_s\downarrow$) at the top of the atmosphere and 1991-2018 mean daily total solar radiation reaching the surface as observed at the BLM site. (b) 1981-2010-monthly averages of snowfall and precipitation, maximum, T_{max}, minimum, T_{min}, and daily mean temperatures, T_{mean}, at the Fairbanks International Airport (PAFA).

the days in November, and from February to April during 1957 to 2008 [32]. According to the 2000 to 2009 radiosonde data, SBI occurred 67% of the time in winter with a mean height of 377 m; SBI occurred with one, two, three, or four simultaneous elevated inversions (EI) in 84.86%, 48.49%, 21.23%, and 7.99% of the 2326 events, respectively [33]. The first EI layer above a SBI formed under anticyclonic conditions at a mean height of 1249 m, under warm-air-advection at a mean height of 1049 m and combined synoptic situations 35.8%, 22% and 23.4% of the time [33].
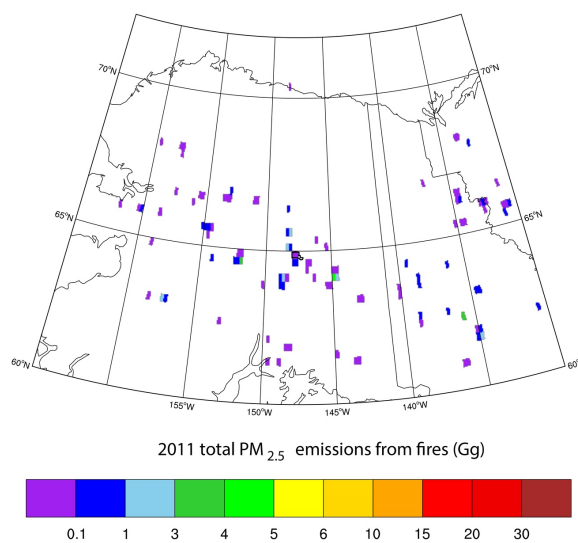
Data from the Global Fire Emission Database [21] showed strong year-to-year variation of annual totals of $PM_{2.5}$ emissions from fires (e.g. **Figures 3(a)-(d)** and **Figure 3(f)**). Fires with low to moderate $PM_{2.5}$ emissions occurred all over Alaska north of 60N in 1999 and 2000. Few fires burned in 2001, 2003, 2006, and 2010 to 2014. In 2002, 2005, 2007 to 2009, and 2015 to 2016, fires occurred in southwest Alaska, the eastern Interior, and along the Alaska-Yukon Territory border. In 2017, most fires burned in the Yukon Flats and Northwest Territory (Canada) (**Figure 3(d)**). Annual totals of Alaska $PM_{2.5}$ emissions from fires exceeded those for anthropogenic sources typically by several orders of magnitude (e.g. **Figure 3**). On average over the area shown in **Figure 3** and 1999-2017, $PM_{2.5}$ emissions from fires were 6985.258 ± 899.813 Gg·y^{-1}. Looking at 1999-2012 (time of overlapping data availability; cf. **Table A1**), mean $PM_{2.5}$ emissions from fires and anthropogenic sources were 378.426 ± 556.718 Gg·y^{-1} and 6.985 ± 0.900 Gg·y^{-1}, respectively.

2004 total PM$_{2.5}$ emissions from fires (Gg)

(a)

2009 total PM$_{2.5}$ emissions from fires (Gg)

(b)

2011 total PM$_{2.5}$ emissions from fires (Gg)

(c)

2017 total PM$_{2.5}$ emissions from fires (Gg)

0.1	1	3	4	5	6	10	15	20	30

(d)

2004 total anthropogenic PM$_{2.5}$ emissions (metric tons)

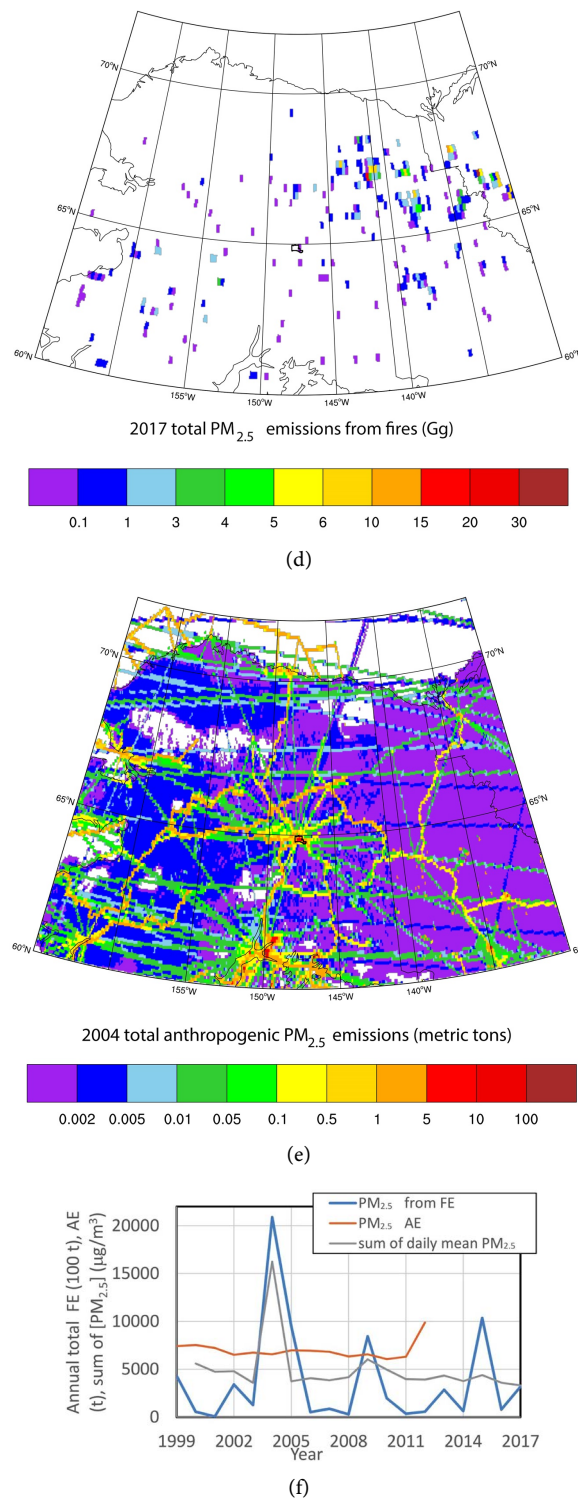|									
0.002	0.005	0.01	0.05	0.1	0.5	1	5	10	100

(e)

(f)

Figure 3. Examples of the spatial distribution of annual total PM$_{2.5}$ emissions between 60N and 72N, 165W and 130W in (a) 2004, (b) 2009, (c) 2011, (d) 2017 from fires and (e) 2004 anthropogenic sources. Units differ among panels due to the large differences. Fairbanks is at 64.84N, 147.72W. (f) Annual total anthropogenic (AE) in metric tons and fire emissions (FE) 100 metric tons in the domain shown in (a)-(e) and annual sum of daily mean [PM$_{2.5}$]. Units differ among curves due to the large differences. Note that 1 Gg = 1000 metric tons.

The 1999-2017 annual mean [PM$_{2.5}$] was 13.2 ± 25.8 μg·m^{-3}, *i.e.* below the current annual mean NAAQS of 15 μg·m^{-3}. At a daily-scale, inter-annual variability was high, especially in summer (**Figure 4**). Cold and warm season [PM$_{2.5}$] were 16.8 ± 12.2 μg·m^{-3} and 11.5 ± 40.9 μg·m^{-3}, respectively (**Table 1**). As indicated by the standard deviations, summer maximum concentrations can exceed winter maximum concentrations by more than an order of magnitude depending on the severity of upwind fires; worst air-quality conditions occurred due to advection of pollutants from wildfires, not anthropogenic emissions trapped under winter surface-inversions. Data from the first tribal-owned air-quality network in the Yukon Flats showed similar behavior [34].

The high standard deviations of concentrations (**Table 1**) have various reasons. In summer, a huge year-to-year variability exists for the location of fires relative to the sites, in the area burned (cf. **Figure 3**), the number of lightning strikes, the type of synoptic scale weather pattern, the levels at which the smoke is transported and the kind of fuel burned. In winter, emissions differed strongly between mild and extremely cold episodes, the number of Chinook situations, as
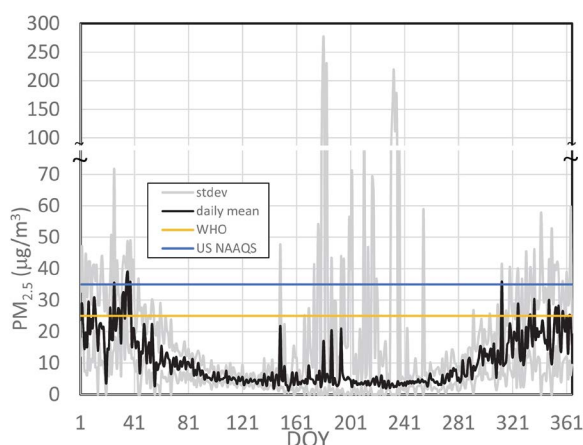

Figure 4. Composite of 10/1/1999 to 3/31/2018 Fairbanks daily mean PM$_{2.5}$ concentrations and 19-year standard deviations of daily means. Legend is interrupted between 70 and 100 μg·m^{-3} and changes spacing. The World Health Organization (WHO) and US EPA recommended 24-h thresholds of 25 μg·m^{-3} [35] and NAAQS of 35 μg·m^{-3} not to be exceeded [36] are superimposed.

Table 1. Means and higher moments of statistics of [PM$_{2.5}$] for 2/1999 to 3/2018.

| Time frame	[PM$_{2.5}$]			
	Mean (μg·m^{-3})	Standard deviation (μg·m^{-3})	Skewness	Kurtosis
All years	13.2	±25.8	11.4	175
Cold season	16.8	±12.2	1.7	6
Warm season	11.5	±40.9	8.5	81

well as under anticyclonic vs. cyclonic conditions. Concentrations strongly varied with inversion duration and surface inversion height.

The different distributions around the means (skewness) of the warm and cold season [PM$_{2.5}$] of 8.5 and 1.7 were due to its different sources and particle age (Table 1). Aerosols are formed and change during transport [11] [37]. The warm season kurtosis of 81 represents the outliers due to inter-annual variability of fires. In Fairbanks, fires made up about 33%, 60%, 83%, 43%, 9%, 25%, 57% and 9% of the events with 24 h-mean [PM$_{2.5}$] greater than 35 µg·m^{-3} in 2000, 2002, 2004, 2009, 2010, 2013, 2015, and 2017, respectively.

3.2. Decadal to Seasonal Scale Impacts

Previous work showed that there was a shift from a cooler to a warmer regime in 1976 [38]. Figures 5(a)-(d) show the monthly mean 2-m air temperatures at the Fairbanks International Airport for November, December January, and February 1930-2018. The linear temperature trends for 1930 to 1975 indicated a slight to notable decrease in the monthly mean 2-m air temperatures for these months. The same was true for 1977 to 2014/15 except February, when the linear temperature trend showed a slight increase. For 1977 to 2018, however, monthly mean 2-m air temperatures decreased only in November and January. All four panels show the 1976 shift from a cooler to a warmer regime. At that time, the PDO index switched from mainly negative to mainly positive values (Figure 5(e)).

These results mean that a regime shift like in 1976 would require less heating, especially in January. Since no [PM$_{2.5}$] monitoring existed before 2/1999, we examined the 1-in-3-days [PM$_{2.5}$] for November, December 1999-2017, January 2000-2018, and February 1999-2018. In those months, [PM$_{2.5}$] decreased on average 1.7, 5.1, 3.2 and 1.1 µg·m^{-3}·decade^{-1}, respectively (Figures 6(a)-(d)). November, December and January monthly mean [PM$_{2.5}$] and PDO showed weak, but significant, negative correlation, while February showed weak, but significant positive correlation (Table B1).

(a)
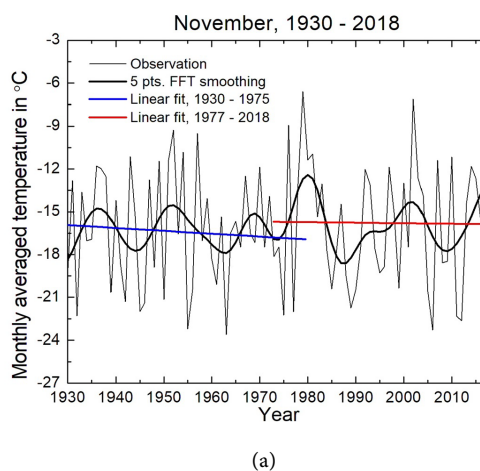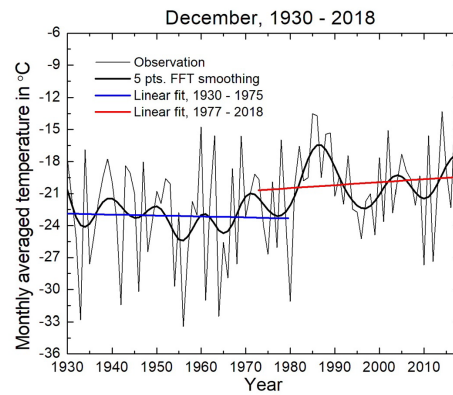
(b)
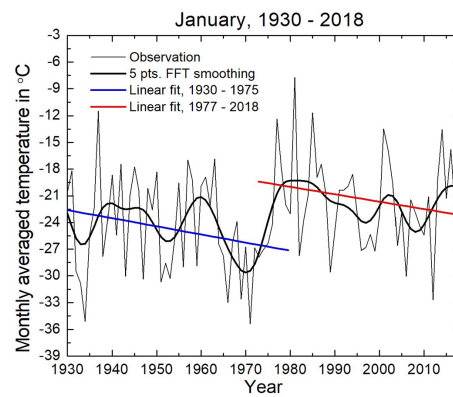
(c)
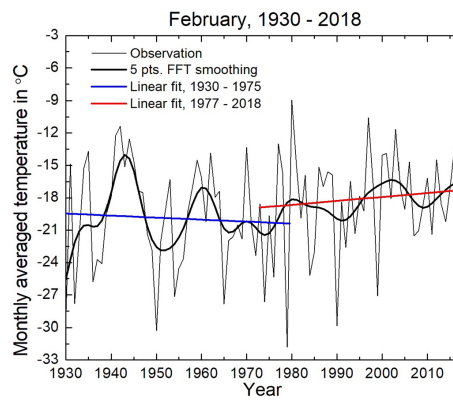
(d)
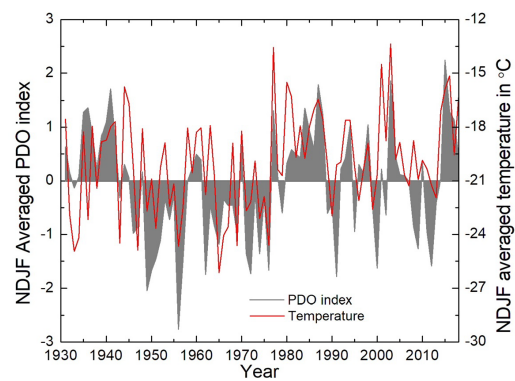
(e)
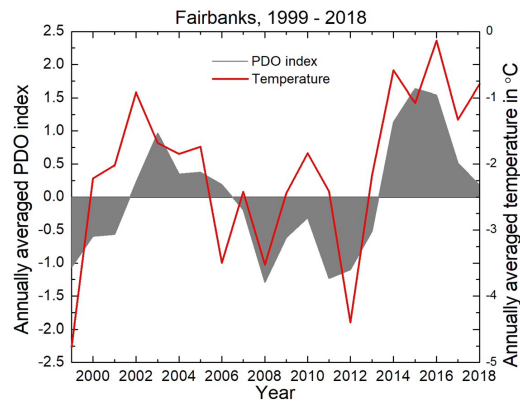
(f)

Figure 5. Monthly mean 2-m temperatures observed at the Fairbanks International Airport (PAFA) between 1929 and 2018 in (a) November, (b) December, (c) January, and (d) February. Red and blue lines are the linear temperature trends for 1929/1930 to 1975 and 1977 to 2018. (e) November, December, January and Februray means of PDO index and 2-m temperatures for 1930-2018. (f) Annually mean PDO and 2-m air temperatures for 1999 to 2018.

(a)

(b)

(c)

(d)

(e)

(f)
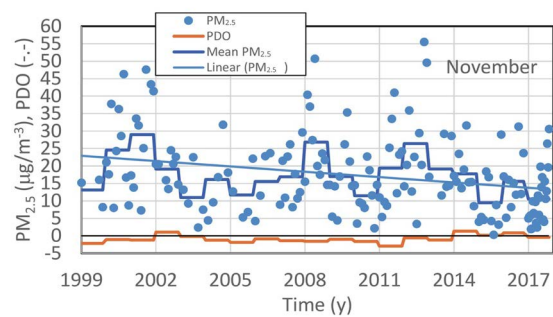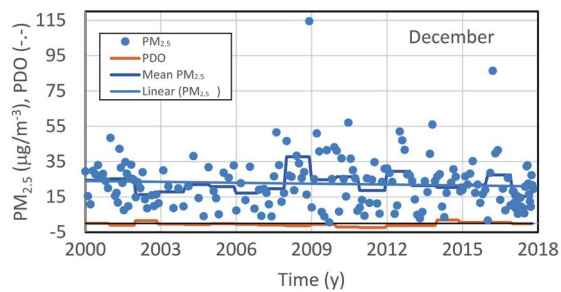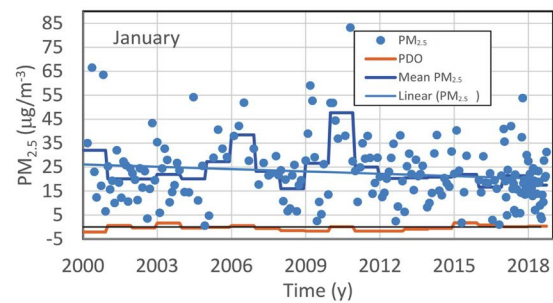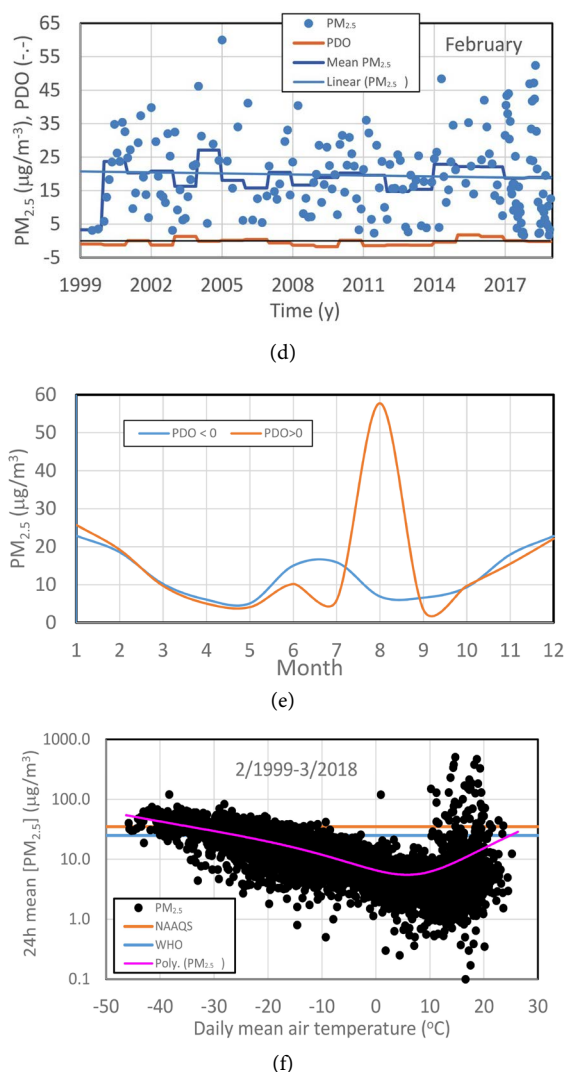
Figure 6. Temporal evolution of 1-in-3-days 24-h mean (dots) and monthly mean [$PM_{2.5}$] (dark blue line), monthly PDO index (orange line) and linear trend line (light blue line) for (a) November, (b) December, (c) January, and (d) February at Fairbanks. Linear trends are with respect to the daily values. Legends differ among panels. (e) Annual course of monthly mean [$PM_{2.5}$] over all months with negative (blue) and positive (orange) monthly PDO-values. (f) 2/1999 to 3/2018 24-h mean [$PM_{2.5}$] vs. daily mean 2-m air temperatures at the BLM site. Y-axis has a logarithmic scale. The pink line represents the 4th order polynomial of $y = 8 \times 10^{-6} x^4 + 0.0006x^3 + 0.0241x^2 - 0.341x + 6.554$ with $R^2 = 0.149$.

In the 2/1999 to 3/2018 timeframe, monthly mean PDO was more often negative than positive. The same was true for annual mean PDO (Figure 5(f)). Cold season monthly means of [$PM_{2.5}$] and PDO had weak, positive, but significant correlation (Table B1). The same was true for the warm season.

Years with negative annual mean PDO had 4.1 μg·m^{-3} higher annual mean [$PM_{2.5}$] than those with positive. Whether on the monthly scale, the PDO phase caused increases or decreases in monthly mean [$PM_{2.5}$] differed in the annual course (Figure 6). On average, cold season mean [$PM_{2.5}$] was 1.8 μg·m^{-3} higher

for positive than negative PDO (Table B2). Warm season mean [PM$_{2.5}$] was 3.1 µg·m^{-3} higher for positive than negative PDO (Table B2). Wildfires and subsidence inversions occur more often in warm than in cool summers. Subsidence inversions reduce the volume in which pollutants accumulate. This means that even when there were no emissions the mass of pollutants per cubic meter increased (see also section 3.6). Consequently, warm season mean [PM$_{2.5}$] increased.

Positive correlation between temperature and PDO and the negative correlation between temperature and emissions together with the trend of decreasing temperature (e.g. Figure 5(d)) suggest some caution in drawing conclusions about attainment or non-attainment. For example, the sudden PDO shift in 1976 went along with an increase of monthly mean temperature up to more than 6 K (Figure 5(c)). However, monthly mean [PM$_{2.5}$] decreased non-linearly with increasing monthly mean temperature until 10°C or so was reached (Figure 6(f)). Thus, looking at just five years in assessing the success/failure of emissions-control measures and deciding on compliance might be too short in regions where a sudden shift in regime like in 1976 may occur.

Looking at 2/1999 to 3/2018, no significant correlation existed between monthly means of NP and [PM$_{2.5}$]. However, in November and December, NP and [PM$_{2.5}$] had moderate, but significant correlation (Table B1). In January and February, weak, negative, but still significant correlations existed. Marginal and weak (both significant at 95% confidence or higher), negative correlations occurred during the warm and cold season, respectively (Table B1).

During 2/1999 to 3/2018, mean [PM$_{2.5}$] were 19.8, 2.1, 8.0 and 3.2 µg·m^{-3} for months with NP < 1000, 1000 ≤ NP < 1010, 1010 ≤ NP < 1020, and ≥1020 hPa, respectively. These findings suggest that a strong northward migration of the polar front with strong ridges over Alaska as well as low pressure systems over the North Pacific both provided favorable synoptic scale conditions for poor air quality in the FMA (Figure 7(a)). Since the FMA is at the northeastern edge of the area for which the NP is defined, low pressure over the North Pacific means that the FMA is influenced by the semi-permanent Canadian High. In both cases, subsidence inversions contributed to low air quality. On average, annual [PM$_{2.5}$] was 5.5 µg·m^{-3} higher in years with NP < 1012 hPa than other years (Table B2). In the former case, the weather in the FMA was governed more often by the semi-permanent Canadian High, *i.e.* storms passed farther south; while in the latter case, the Hawaiian High was strong shifting the tracks of Aleutian Lows northward.

During 2/1999 to 3/2018, annual mean [PM$_{2.5}$] was 3.6 µg·m^{-3} lower in years with positive than negative SOI (Table B1). In months with positive SOI, monthly mean [PM$_{2.5}$] were on average 2.5 µg·m^{-3} lower than in months with negative SOI (Figure 7(b)).

On average over 1999-2018, monthly mean [PM$_{2.5}$] decreased with increasing monthly mean temperatures up to about 10°C and increased steeply above this
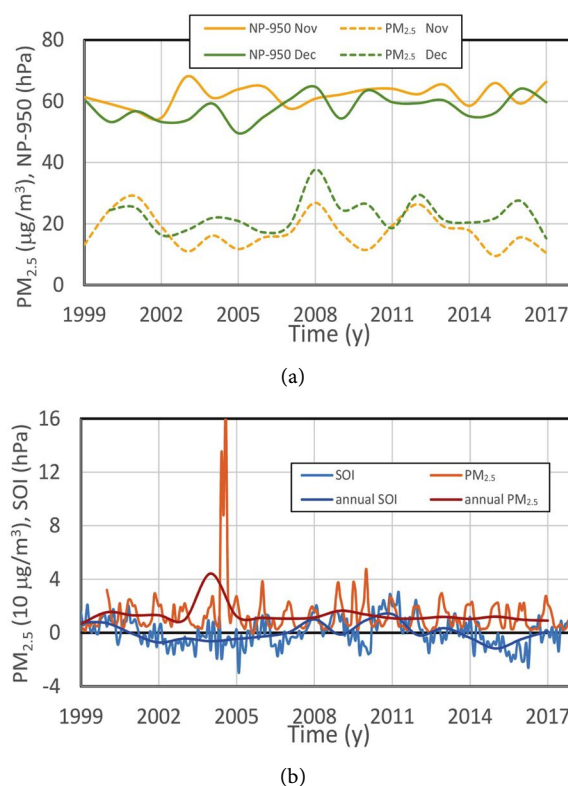
(a)

(b)

Figure 7. November and December 1999-2017 climatology of (a) monthly means of NP-950 hPa and [$PM_{2.5}$], and (b) monthly and annual means of SOI and 0.1 [$PM_{2.5}$].

value (cf. **Figure 6(f)**). Typically, monthly mean [$PM_{2.5}$] increased with increasing monthly means of relative humidity due to swelling of aerosol under wet conditions. The increase was steepest for monthly means of minimum relative humidity.

At the State Office Building (SOB), in all years and on 2005-2014 average, carbon (OC + EC) contributed the most to the total [$PM_{2.5}$], followed by sulfate. Carbon, sulfate, ammonium, nitrate, non-metals and metals made up about 37%, 34%, 14%, 10%, 4% and 1% of the $PM_{2.5}$, respectively. The 2005-2014 (some missing data) mean $PM_{2.5}$ (9.9 ± 12.2 µg·m^{-3}) composition included about 0.6 ± 0.6 µg·m^{-3} nitrate, 0.8 ± 1.1 µg·m^{-3} ammonium, 0.9 ± 0.9 µg·m^{-3} elemental carbon, 4.7 ± 6.2 µg·m^{-3} organic carbon, 1.8 ± 2.1 µg·m^{-3} sulfate, 0.4 ± 0.3 µg·m^{-3} metals and 0.7 ± 0.8 µg·m^{-3} non-metals, *i.e.* inter-annual variability of species was of similar magnitude than their means. The reasons were the same as already discussed for the inter-annual variability of daily mean [$PM_{2.5}$].

Except for metals, the 2005-2014 speciation climatology showed distinct seasonality and annual courses (**Figures 8(a)-(e)**) due to the different emissions sources, their strengths and fractional contribution to emitted $PM_{2.5}$ and precursor gases as well as weather conditions. Interestingly, significant correlation (95% confidence or higher) existed between sulfate, ammonium and non-metals (**Figure 8(f)**). Except metals and OC, all $PM_{2.5}$ species concentrations increased as temperatures decreased in fall, peaked in January (coldest month), and de-

creased as temperatures increased (compare Figure 2(b), Figure 8(e)). Organic carbon had a secondary peak in July due to fires and small contributions from biogenic emissions. Its concentrations were smallest in late spring and early fall. In late spring, the fire season has not yet started and spatial heating by wood is already reduced. In early fall, the fire season is already over or slowing down and space heating is still sparse.

Non-metals hardly varied among years for April to September and year-to-year differences were largest in December (Figure 8(e)). EC showed lowest inter-annual variability in April and May, and slight variability in summer. In fall, EC inter-annual variability increased to peak in December. OC showed largest inter-annual variability in August due to rain and second largest in December. OC barely varied among years during breakup (April, May).
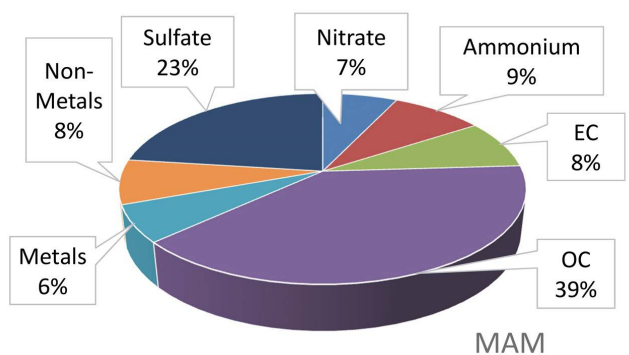
(a)
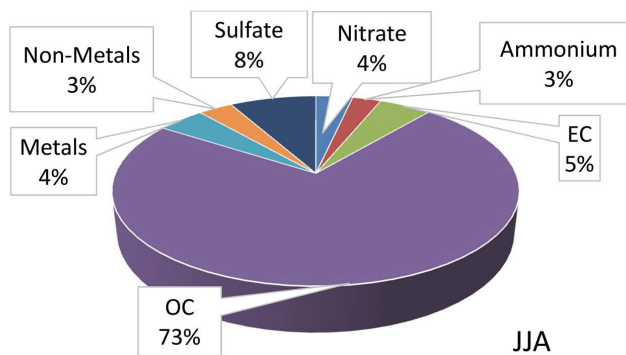
(b)
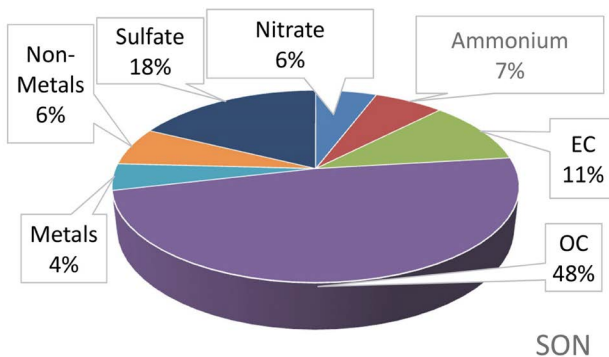
(c)
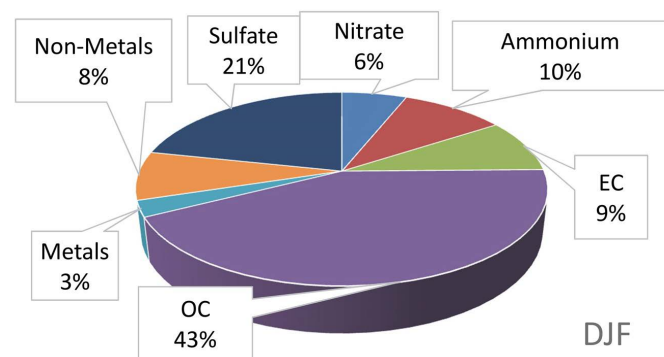
(d)
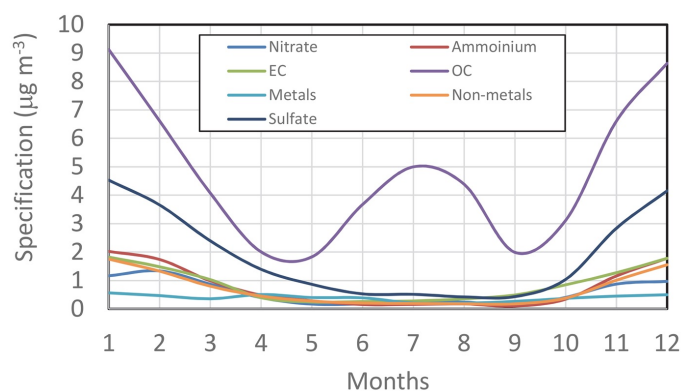
(e)
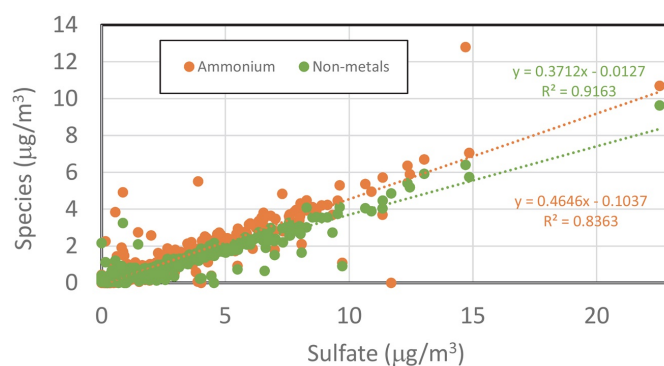
(f)

Figure 8. Fairbanks 2005-2014 1-in-3-days mean [$PM_{2.5}$] speciation climatology (a) spring, (b) summer, (c) fall, (d) winter, (e) mean annual course and (f) correlation between sulfate and non-metals as well as ammonium.

Inter-annual variability of nitrate and ammonium peaked in February with NH_4 varying strongest. A small secondary peak occurred in August. Both [NO_3] and [NH_4] varied least among years from April to June and in September. While in the cold season, monthly means and inter-annual variability of [NO_3] were lower than for [NH_4], the opposite was true in the warm season. Sulfate varied strongest among years in December, and least from April to September. This behavior hints at oil-fired furnaces and temperature being major influences for inter-annual variability of sulfate.

The lower [NH_4] in summer than all other seasons ([Figures 8(a)-(e)](#)) can result from hydro-thermodynamic-caused shifts in the system HNO_3-NH_3-NH_4NO_3-sulfate. When air temperature rises above 15˚C and relative humidity decreases below 60% on sunny summer days under high nitric acid (HNO_3) to ammonia (NH_3) ratios ($HNO_3/NH_3 > 3$), ammonium nitrate (NH_4NO_3) dissociates to NO_3^- and NH_4^+ particles, and HNO_3 is in the gas phase [39] [40].

Thermodynamic conditions cooler and wetter than 14˚C and 60%, respectively, limit the chemical reactions of the system [39] [40]. They favor ammonium-nitrate formation on sulfate- and/or carbon-dioxide-containing particles. When the concentrations of the latter particles is high (35 - 85 µg·m^{-3}), the [HNO_3] and [NH_3] decrease [39] [40].

Metals showed a non-linear relationship to relative humidity in January, April, May, and November.

For all years, only monthly total insolation at the surface showed a notable (R^2 = 31%) correlation with monthly mean [$PM_{2.5}$] ([Table B3](#)). During winter, metals, sulfate, nitrate, and OC had a nonlinear relationship with solar radiation reaching the surface. In winter, when insolation and temperatures are low ([Figure 2](#)) burning of old motor oil for heating of shops releases metals. The rest of the species showed a linear relationship during summer and winter. In winter, emissions from cold starts, driving short distances and heating increase [NO_2], [SO_2] and [OC]. At below freezing temperatures and high relative humidity (> 70%), NO_2, SO_2, and NH_3 are taken up in super-cooled droplets. Here non-linear aqueous phase processes occur [11] [37]. Typically, kinetic rate constants increase exponentially.

In the cold season, monthly total solar radiation at the surface, and monthly means of wind speed, 2-m air temperature, maximum and minimum temperatures correlated negatively, moderately to weakly with mean [$PM_{2.5}$], but at 95% or higher confidence ([Table B3](#)). Species concentrations were higher at low wind speeds in winter than in summer. In the warm season, monthly means of 10-m wind speed and [$PM_{2.5}$] correlated the strongest. However, the paired two-tailed t-test indicated a 95% probability of an accidental correlation.

Monthly mean maximum fuel temperature was weakly, and monthly mean minimum relative humidity was negatively correlated with [$PM_{2.5}$]. Both correlations were significant at 95% confidence. Low relative humidity during April and September promoted increased [$PM_{2.5}$]. Low moisture enables more efficient radiative cooling, formation of temperature inversions and therefore, accumulation of emitted pollutants. Monthly accumulated precipitation and mean [$PM_{2.5}$] as well as daily soil moisture and [$PM_{2.5}$] were uncorrelated. The latter confirms that uptake of soil material by wind seldom contributed to [$PM_{2.5}$] in the FMA.

EOF analysis is strictly mathematical [29], *i.e.* it is not statistical and not based on physics. It provides orthogonal time series and orthogonal patterns. The latter are a function of the variable domain. Since they may resemble physical modes of the system, we computed EOFs with a correlation matrix [30] using

the 2010 to 2017 daily $[PM_{2.5}]$ and meteorological quantities by removing the appropriate means and calculating the correlation matrix using anomalies. This analysis revealed the following: In the annual course, the eigenvalues of the first EOF for relative humidity were positive when those for temperature were negative and vice versa except for November to February. During these month, temperature and relative humidity eigenvalues verified the same sign, but opposite to the sign of the $PM_{2.5}$ eigenvalues. In March and October, the signs of the temperature, wind speed and insolation eigenvalues were positive, while those of relative humidity and $PM_{2.5}$ were negative. In April and September the opposite was true. Except for May to July eigenvalues of wind speed and insolation were of same sign either positive or negative.

The first three EOFs of daily total insolation, means of temperature, wind, relative humidity, and $[PM_{2.5}]$ explained 57%, 17% and 15% of the data. This finding suggests that external forcing by insolation and by synoptic-scale conditions on mesoscale features like radiation inversions and subsidence inversion governed the air quality of the FMA. Plots of the first EOF-eigenvalues of $PM_{2.5}$ vs. other meteorological variables suggested little impact of relative humidity on $[PM_{2.5}]$. On the monthly scale, the first EOF varied among months explaining between 37% and 51% of the data. On the seasonal scale, the first EOF explained 39%, 56%, 42%, and 56% of the data in DJF, MAM, JJA and SON, respectively. This means drivers for air quality differed among seasons.

We also calculated the EOFs by removing the appropriate means and calculating the covariance matrix using anomalies. To normalize the EOFs to one, we divided them by the square root of the associated eigenvalue [30]. Multiplication with 100% provides the percentage attributed to the respective EOF. The first, second and third EOF of 2010 to 2017 daily means of insolation, temperature, wind, relative humidity, and $[PM_{2.5}]$ explained 94%, 5% and less than 1% of the data. On monthly scale, the first EOF varied among months explaining between 49% and 98% of the data. The first EOF had the largest eigenvalues for insolation except for June, July and December when they were negative. On seasonal scale, the first EOF explained 49%, 98%, 81%, and 90% of the data in DJF, MAM, JJA and SON, respectively. Together these results mean that DJF $[PM_{2.5}]$ is hardest to predict.

On the cold seasonal scale, the FFT revealed that high mean $[PM_{2.5}]$ coincided when the first and second amplitude were in sync and the third was in sync or at least high.

3.3. Impact of Daily Meteorological Conditions

Wildfire smoke impacts the radiation budget [41]. Over 2/1999 to 3/2018, daily $[PM_{2.5}]$ showed weak, negative, but significant correlation to daily total solar radiation at the surface (Table B3). At daily mean temperatures below −20°C, $[PM_{2.5}]$ were clustered below 20 µg·m^{-3} (e.g. Figure 6(f)). Warm season daily mean $[PM_{2.5}]$ were clustered below 5 µg·m^{-3} for temperatures below 10°C.

On 2005-2014 average, 1-in-3-days ammonium, sulfate, EC, OC and non-metals concentrations correlated significantly and negatively with daily mean temperatures (Table B3). Correlation with daily minimum temperatures was significant for all species at 95% confidence. Except for [OC] the same was true for daily maximum temperatures. In the cold season, even though the correlations were low, all 1-in-3-days species correlated with 95% confidence with daily mean, minimum and maximum temperatures. Except nitrate, species concentrations correlated the highest with daily mean 2-m temperatures followed by minimum and maximum 2-m temperatures. Nitrate correlated the strongest with daily maximum temperatures (-0.364). In the warm season, a marginal, positive, but significant correlation existed between daily maximum temperatures and metals, and for [OC] with daily mean and minimum temperatures (Table B3).

A strong correlation existed between temperatures below $-20°C$ and some $PM_{2.5}$ species (Table B3). Here sulfate was prominent due to increased emissions of primary sulfate and SO_2 precursors from power generation and heating. As temperature increases, gas-to-particle conversion slows down [37].

At high relative humidity, the uptake of water vapor by aerosols promoted particle growth. Thus, [$PM_{2.5}$] decreased as particles shifted towards diameters larger than 2.5 μm. Ammonium and sulfate peaked at lower daily mean relative humidity than nitrate. The fraction of metals thrived during April and September on days when relative humidity was less than 75%.

In winter, species concentrations were higher (up to 4 μg·m^{-3} for all species, except sulfate with a maximum of about 10 μg·m^{-3}) under calm wind conditions than for wind speeds ≥ 0.5 m·s^{-1}. Ammonium showed a linear relationship with wind speed, while non-metals, EC, sulfate, metals, and OC showed nonlinear relationships. Nitrate had a distinct nonlinear relationship with wind speed during December. Of course, the chemical hydro-thermodynamic processes of the system HNO_3-NH_3-NH_4NO_3-sulfate partly played a role. In addition, as wind speed increases, so does mixing. Segregation close to emission sources that may limit chemical hydro-thermodynamic processes [42], has less impact on the reactions at high than low wind speeds [42].

We calculated the correlation between wind directions and concentrations using all available wind direction data, *i.e.* not individual wind-direction sectors. No significant correlation was found except for NO_2 with R = -0.179 (Table B3). Nitrate barely depended on wind direction, while ammonium and sulfate both peaked in the sectors 135° - 225° and 270° - 340° (Figure 9(d)). At all sites, also [$PM_{2.5}$] increased when wind came from these directions (Figure 9(e)). Interestingly, cold season [O_3] was low for these sectors as well. In these broader sectors, the only potential sources for ammonium- and sulfate-aerosol precursors are NH_3 and hydrogen sulfide (H_2S) emitted from hot springs. The formation of SO_2 from H_2S destroys O_3 [43] (see Section 3.5 for details).

Sulfate has a higher mass than nitrate causing the fraction of $PM_{2.5}$ to increase

(a)

(b)

(c)

(d)

(e)

(f)

(g)
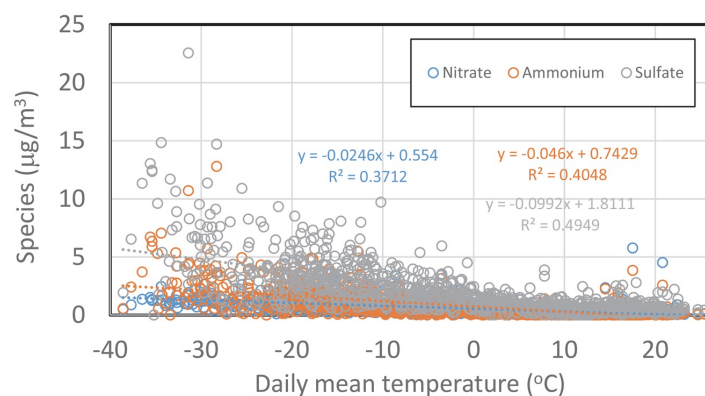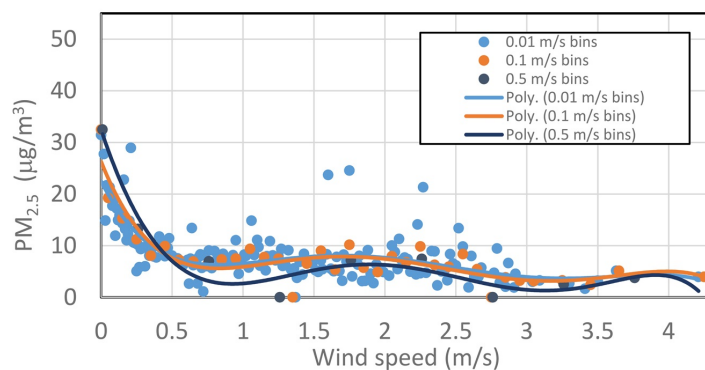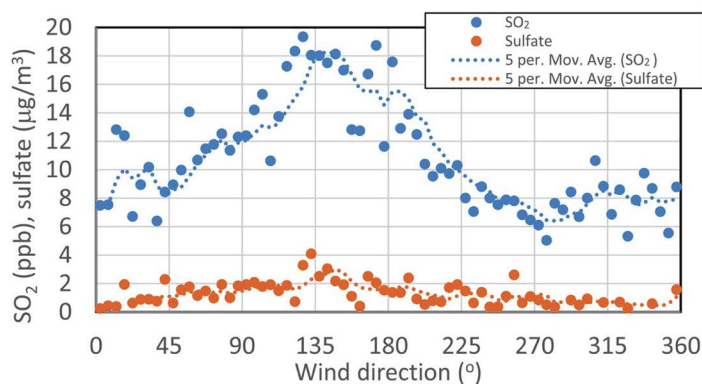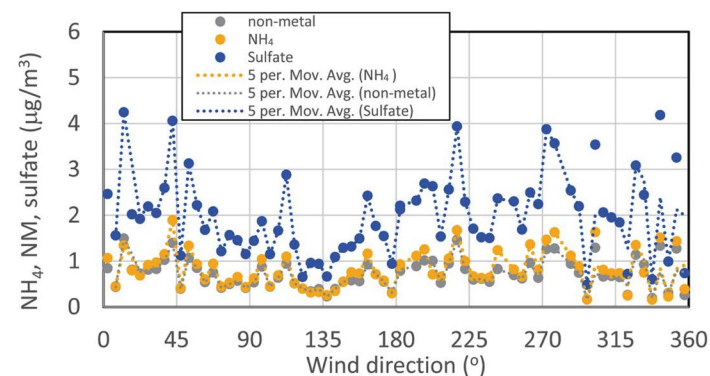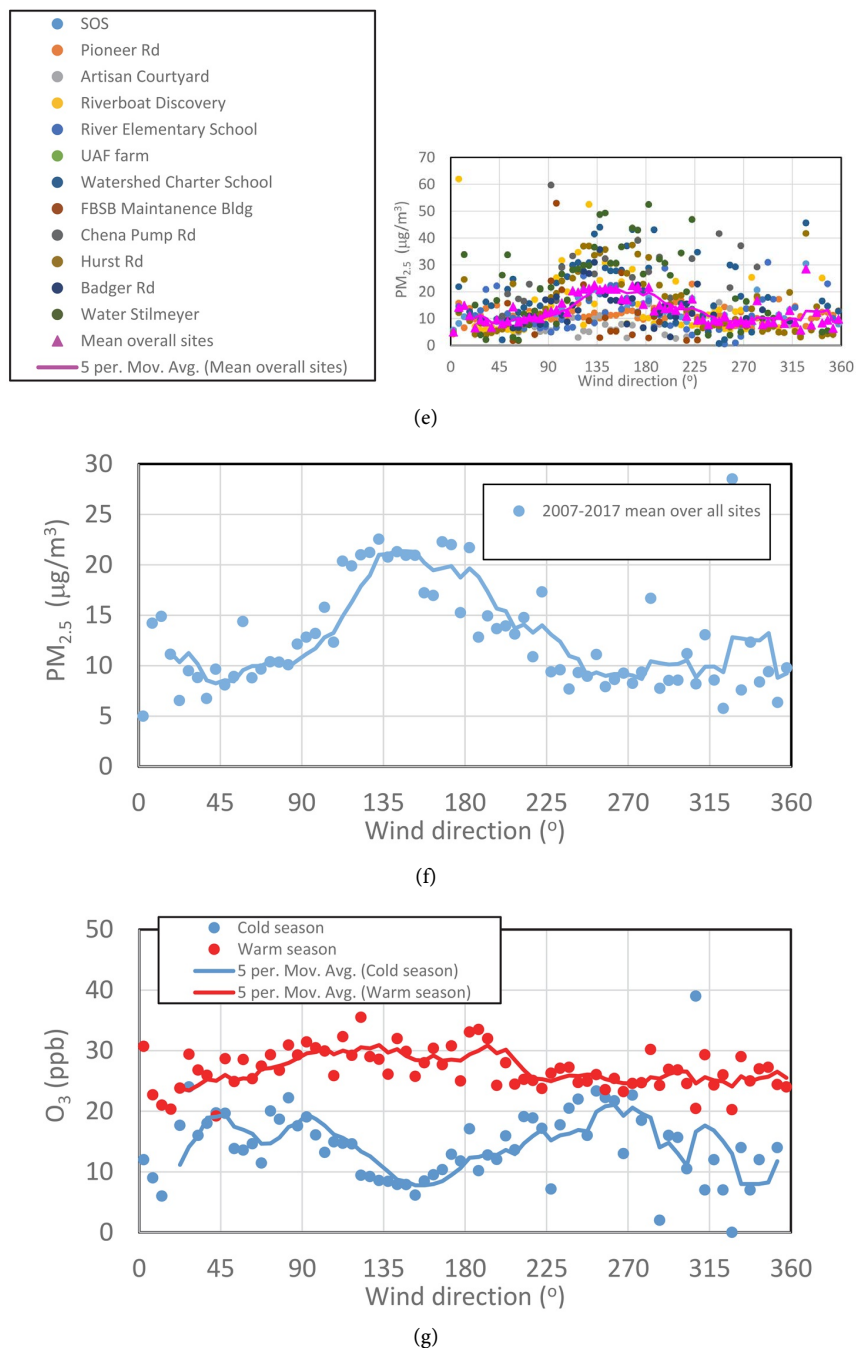
Figure 9. 2005-2014 mean speciation of $PM_{2.5}$ and $PM_{2.5}$ relationships to meteorology of (a) selected species vs. temperature, (b) 2007-2018 $PM_{2.5}$ from all sites vs. mean wind speed in 0.01, 0.1 and 0.5 m·s^{-1} bins and respective polynomial fits (lines) of $y = -0.608x^5 + 7.3687x^4 - 32.671x^3 + 64.099x^2 - 54.139x + 22.49$, $y = -0.7683x^5 + 9.3061x^4 - 41.213x^3 + 80.951x^2 - 68.613x + 26.253$, $y = -0.2393x^6 + 2.0569x^5 - 2.6148x^4 - 21.151x^3 + 74.983x^2 - 82.772x + 32.427$ with R^2 of 0.512, 0.808, 0.940, (c) 2011-2014 SO_2, sulfate vs wind direction in 5° sector bins, (d) 2005-2014 climatology of nitrate, sulfate, and non-metals (NM) vs. wind direction in 5°-sector bins, (e) 2007-2017 $PM_{2.5}$ at all sites in the FMA and mean over all sites as function of wind direction in 5°-sector bins, (f) 2007-2017 mean $PM_{2.5}$ averaged over all sites in the FMA as a function of wind direction. (g) Warm and cold season O_3 vs. wind direction. Lines are 5-values running means.

proportionally with increasing fraction of sulfate. Comparison of the average $[PM_{2.5}]$ with its fraction without NO_3 revealed that the latter was much lower during winter than summer. This means that wood stoves are major contributors of nitrate and secondary aerosols formed from nitrogen oxides and other fine particulate matter.

A nonlinear relationship with temperature occurred for nitrate in February, April, October, and December, for sulfate from November to February and in April, for ammonium from January to March, and for metals from December to March. A nonlinear relationship with temperature existed for metals from May to August. Sulfate increased when temperatures were below −20°C. Nitrate, ammonium, sulfate, EC and non-metal concentrations correlated about 37%, 40%, 49%, 30% and 46% with temperature (Table B3). Below 10°C, OC increased with decreasing daily mean temperature. This behavior is due to increasing emissions from space heating as temperatures drop. Above 10°C, OC increased with daily mean temperature which can be explained by increasing emissions from wildfires. In August, the rainiest month (Figure 2(b)), rain over several days and decreasing temperatures may lead to onset of space heating. The amount of metals increased when relative humidity was less than 75%.

Precipitation showed weak negative, but significant correlation with NO_2, O_3, SO_2, CO and $PM_{2.5}$ (Table B3) due to uptake into drops, washout and scavenging.

3.4. Spatial Distribution

Mobile $[PM_{2.5}]$ measurements and measurements performed at various sites for a cold season or more, revealed the impact of local emissions [44]. Figure 10 displays a spatial composite of cold season mean $[PM_{2.5}]$ from measurements at the sites. Note that mobile measurements suggested an additional hot spot between Fairbanks and North Pole [44] [45].

The $[PM_{2.5}]$-relative humidity relationships differed among sites (Table 2). At the Hurst Rd (HR), Riverboat Discovery (RD), SOB and Badger Rd (BR) sites, negative and positive correlation existed for maximum and minimum relative humidity, respectively, and mean relative humidity showed no correlation except at the RD site. Unlike for most sites, at the RD site, measurements continued over summer to assess the impact of ship emissions. June 1 to September 15, 2013, 24 h-mean $[PM_{2.5}]$ was 11.4 µg·m^{-3}.

At the Water Stillmeyer (WS) and Wood River Elementary School (WRES) sites, $[PM_{2.5}]$ increased when relative humidity decreased and vice versa (Table 2). This means coarse particles greater than 2.5 µm in diameter shrunk and contributed to $[PM_{2.5}]$ as relative humidity decreased. Once relative humidity increased particles grew to greater than this threshold contributing to particulate matter of 10 µm in diameter or less. This finding suggests that the dry aerosol was relatively large in diameter. In the WS and WRES neighborhoods, wood burning dominated.
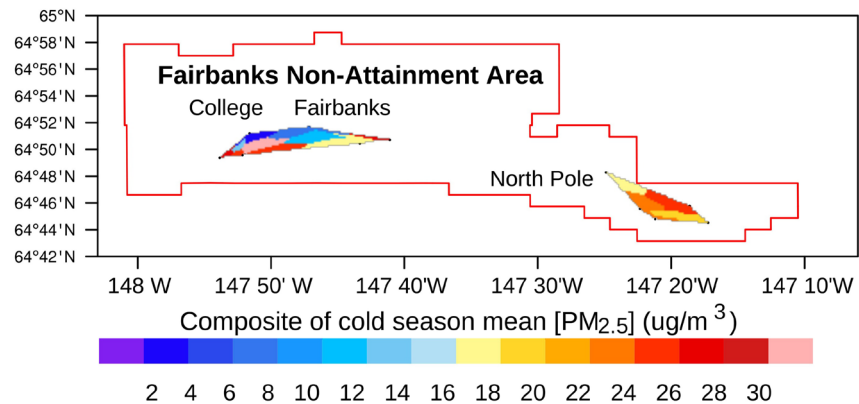
Figure 10. Composite of spatial distribution of cold season mean [PM$_{2.5}$] observed at the sites (black dots) in the FMA. The red polygon shows the non-attainment area.

Table 2. Correlation coefficients, R, of daily accumulated short-wave downward radiation received at the surface R$_s$↓, daily mean 2-m T, maximum T$_{max}$ and minimum T$_{min}$ air temperatures as well as daily mean, maximum and minimum relative humidity RH, RH$_{max}$, RH$_{min}$, daily mean wind speed v, gust wind speed v$_{gust}$, and wind direction, dir observed at the BLM site with 24 h-mean [PM$_{2.5}$] at selected sites in the FMA since 1/1/2007. Bold values indicate significant correlations at 95% confidence according to a pair two-tailed t-test. All available data were used, *i.e.* correlations represent different observation periods and sample sizes (See Table A2 for details). SOB, PR, AC, WCS, RD, WRES, CPR, HR, BR, and WS are the State Office building, Pioneer Rd, Artisan Courtyard, Watershed Charter School, Riverboat Discovery, Wood River Elementary School, Chena Pump Rd, Hurst Rd, Badger Rd and Water Stillmeyer sites. See Table B3 for correlation of [PM$_{2.5}$] in the warm and cold seasons. Note that Table B3 lists the correlations for the SOB for 2/1999 to 3/2018.

Quantity	BLM site weather parameter correlation with [PM$_{2.5}$]										
	SOB	PR	AC	RD	WRES	WCS	FMB	CPR	HR	BR	WS
R$_s$↓	**−0.377**	−0.075	**−0.307**	**−0.407**	**−0.410**	**−0.214**	**−0.540**	0.061	**−0.380**	**−0.336**	**−0.304**
v	−0.332	−0.056	**−0.476**	**−0.372**	**−0.446**	**−0.329**	−0.252	**−0.560**	**−0.372**	**−0.410**	**−0.436**
Dir	−0.010	0.012	**0.371**	−0.103	0.158	0.079	−0.180	**0.397**	−0.035	**0.096**	0.144
v$_{gusts}$	**−0.409**	−0.063	**−0.557**	**−0.538**	**−0.515**	**−0.306**	**−0.362**	**−0.602**	**−0.482**	**−0.453**	**−0.514**
T	**−0.532**	**0.034**	**−0.476**	**−0.548**	**−0.741**	**−0.574**	**0.069**	**−0.371**	**−0.579**	**−0.525**	**−0.699**
T$_{max}$	**−0.518**	**0.032**	**−0.476**	**−0.534**	**−0.718**	**−0.522**	**0.034**	**−0.339**	**−0.562**	**−0.450**	**−0.677**
T$_{min}$	−0.507	0.049	**−0.412**	−0.521	−0.644	−0.556	0.199	−0.379	−0.551	−0.427	−0.638
RH	0.034	0.078	0.428	**0.045**	−0.303	−0.425	0.385	0.201	0	**0.136**	−0.305
RH$_{max}$	−0.394	0.032	0.018	**−0.439**	**−0.532**	**−0.476**	0.310	0.103	−0.445	**−0.111**	**−0.578**
RH$_{min}$	0.226	0.045	0.613	**0.235**	−0.006	**−0.211**	0.304	0.357	0.250	**0.272**	0.050

At the FNSB Maintenance Building (FMB) and Chena Pump Road (CPR) sites, [PM$_{2.5}$] increased with relative humidity. This finding suggests comparatively smaller particles than at WS and WRES. In the WS and WRES area, wood burning dominates space heating.

At all sites, significant correlation existed between [PM$_{2.5}$] and mean temperatures (Table 2). Nevertheless, the correlation was only moderate except for the downtown sites (SOB, PR, FMB) where it was weak-to-marginal. In downtown,

many buildings are heated by steam, *i.e.* increased emissions from spatial heating when temperatures dropped occurred elsewhere. The heat island effect [46] may also be a contributor. For instance, the 2005 October to December mean temperature was 1.8 K higher at the SOB than at the BLM site with a correlation coefficient, R = 0.949. Recall the observations at the BLM site served as a proxy for the synoptic scale conditions.

Absolute values of correlation coefficients, R between meteorological quantities and [$PM_{2.5}$] were the smallest at the UAF experimental Farm (therefore not listed). This site is at the inflow from a clean air-shed. At the FMB site, absolute values of correlation coefficients were low for all meteorological quantities expect daily accumulated radiation (Table 2). Daily mean temperatures correlated the highest with [$PM_{2.5}$] at the WRES and WS sites. In the areas around the WRES and WS sites, wood burning is the major heating source.

3.5. Relations between Reactants of Precursors, Precursors and Particle Species

In the cold season, [O_3] were on average low. Ozone concentrations increased as the length of daylight increased (compare Figure 2(a), Figure 11(a)). The high albedo of snow supported photolysis. From mid-April to solstice [O_3] were typically around 38 ppb. Thereafter, [O_3] decreased as daylight time decreased (cf. Figure 2, Figure 11(a)). In fall, a snow cover temporally can increase photolysis rates leading to a slight increase in [O_3]. This behavior was found also for other high latitude cities [47].

Over the entire period, significant, but weak (R = −0.347) and marginal (R = 0.180) correlation occurred between [$PM_{2.5}$] and [O_3] as well as between [CO] and [$PM_{2.5}$], respectively (Table 3). The negative relationship between [$PM_{2.5}$] and [O_3] is due to the former being the major winter pollutant when insolation and hence ozone formation is low. This means the FMA is a perfect testbed to examine health impacts of [$PM_{2.5}$] without high concentrations of cofounding O_3.

(a)

(b)

(c)

(d)
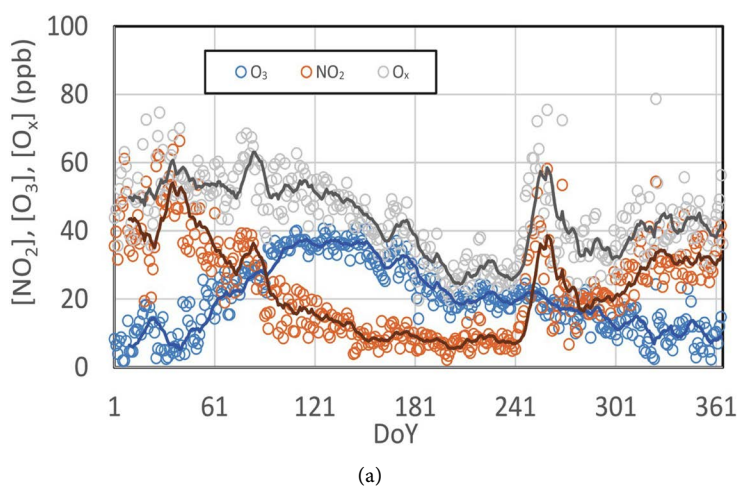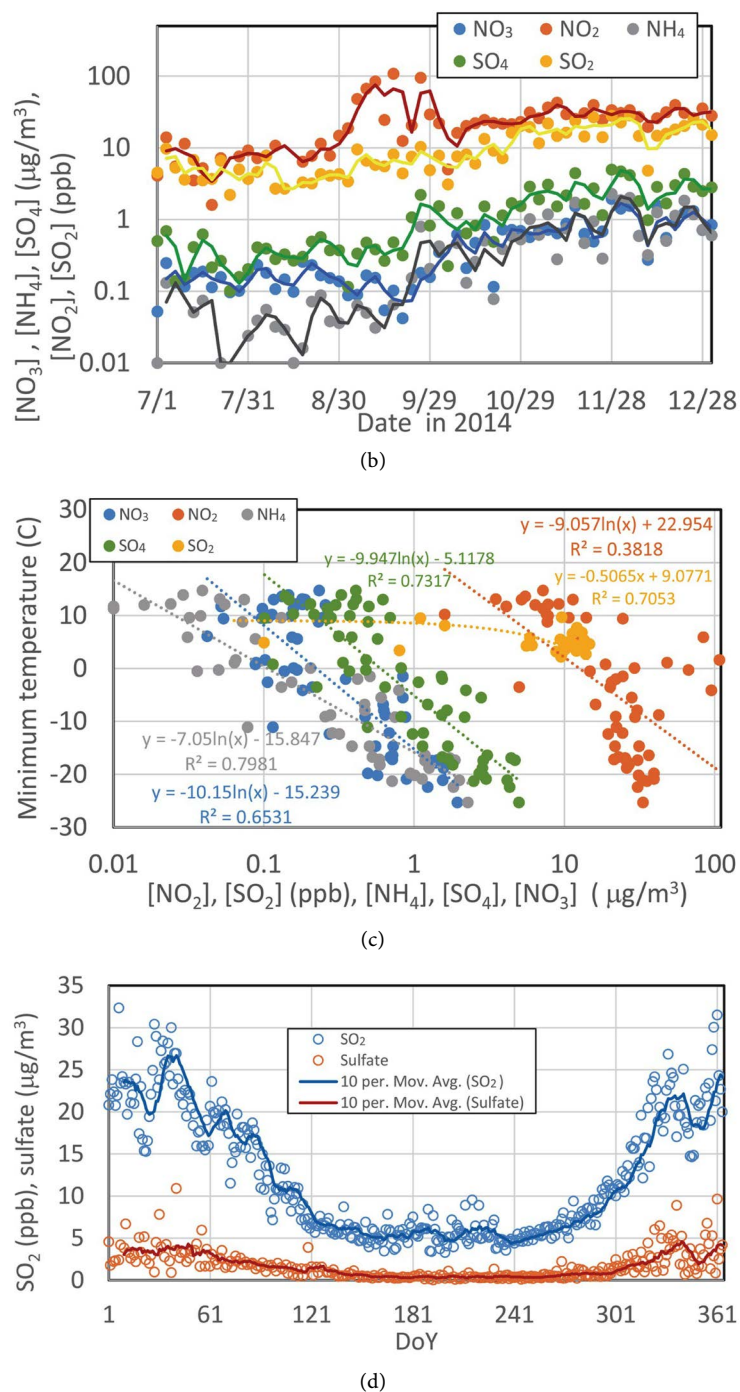
Figure 11. Composites of annual mean courses of precursor gases, selected reactants and aerosols (a) $[NO_2]$, $[O_3]$ and $[O_x]$ where due to lack of other data the simple approximation $O_x \sim O_3 + NO_2$ is adopted. Lines are 10 per moving average. (b) $[NO_2]$, $[SO_2]$, ammonium, nitrate and sulfate for 7/1/2014 to 12/31/2014, the time for which data existed for all five species. Y-axis is logarithmic. All composites encompass data available during overlapping periods of the respective species. (c) $[NO_2]$, $[SO_2]$, ammonium, nitrate and sulfate concentrations as a function of daily minimum temperature with trendlines, their equations and R^2 superimposed. The trend is linear for SO_2, for which the trendline shows curved on the logarithmic X-axis. (d) Annual course of $[SO_2]$ and sulfate concentrations.

Table 3. Correlation coefficients, R, of precursor gases with their aerosols, gases reacting with each other as well as gases co-emitted. To maximize the size of the samples, #, all data for times that a respective pair of species had in common were used. This means that the correlations represent different periods and that the sample sizes differ. For availability of the various species see Table A2. All correlation were significant at 95% confidence or higher according to a paired two-tailed t-test. Correlations and sample size for 7/1/2014 to 12/31/2014 is given in Italic.

Correlations and sample sizes											
Species	$SO_4:SO_2$	$SO_4:NH_4$	$SO_4:O_3$	$SO_2:O_3$	$NO_3:NO_2$	$NO_2:NH_4$	$NO_2:O_3$	$NO_2:CO$	$CO:EC$	$CO:OC$	$NO_3:NH_4$
R	0.666	0.914	−0.369	−0.419	0.120	0.169	−0.401	0.723	0.495	0.581	0.772
#	393	1114	1261	2237	60	56	1713	1287	1350	1353	1117
R	*0.907*	*0.982*	*−0.544*	*−0.427*	*0.120*	*0.169*	*−0.029*	*0.480*	*0.495*	*0.791*	*0.772*
#	*61*	*62*	*60*	*179*	*60*	*56*	*58*	*178*	*62*	*62*	*62*

[NO$_2$] was lowest at the end of August due to scavenging by rain, increased in September due to biogenic emissions from soils and showed a secondary minimum once a snow cover established (compare Figure 2(b), Figure 11(a)). As temperatures dropped, [NO$_2$] increased due to increasing emissions from cold starts and short distance traffic as well as idling of diesel vehicles. [NO$_2$] showed a moderate, negative, but significant correlation with [O$_3$] (Table 3). This finding suggests that due to the high albedo of snow on clear days even despite the low Sun, photolysis dissociates NO$_2$ to O and NO during the short daylight hours. Subsequently, the O reacts with O$_2$ in the presence of a third molecule to form O$_3$. The negative correlation of NO$_2$ vs. O$_3$ may also reflect the role of NO and VOC on O$_3$ near the surface to a certain degree.

Measurements of all precursor gases and aerosols overlapped only for six months (cf. Table A2). Despite NO$_2$ is a precursor to nitrate aerosol, their positive correlation was weak, although significant (Table 3).

Unfortunately, no observation data on NH$_3$, a precursor gas for NH$_4$, were available. Ammonia can neutralize atmospheric acidic substances such as sulfuric acid (H$_2$SO$_4$) and HNO$_3$ [11] [37]. Current qualitative understanding of the ammonium-sulfate-nitrate systems is that NH$_3$ has a greater affinity for H$_2$SO$_4$ than for HNO$_3$. All H$_2$SO$_4$ takes up available 2 NH$_3$ to form ammonium-sulfate ((NH$_4$)$_2$SO$_4$) before any remaining NH$_3$ reacts with HNO$_3$ to ammonium-nitrate (NH$_4$NO$_3$) [37]. This means the heavier (NH$_4$)$_2$SO$_4$ (132 g·mol^{-1}) forms before the lighter NH$_4$NO$_3$ (72 g·mol^{-1}) does.

Important sources of NH$_3$ are life stock, emission from soils due to ammonification of humus, losses of NH$_3$-based fertilizers from soils, and industrial emissions [11]. In the FMA, [NH$_4$] is much higher than expected from the low presence of life stock, agriculture and industry. A study showed that biomass burning in Eastern Europe caused high deposition of NH$_4$ in northern Fennoscandia [48]. Thus, as long as no snow cover exists re-uptake of wildfire-related deposited NH$_4$ might be an unaccounted for source. Another study showed that pets are substantial sources of NH$_3$; dogs, for instance, emit between 0.346 and 1.333

kg NH_3 per year with a mean of 0.974 kg·y^{-1} [49]. In the outskirts of the FMA, many dog kennels exist with often more than ten animals.

On average, daily maximum [SO_2] was larger in winter than summer (**Figure 11(c)**). Mean JJA maximum [SO_2] was 5.4 ppb ranging between 3.3 and 9.5 ppb, while December, January and February values were 21.8, 14.6 and 32.3 ppb, respectively. Mean JJA and DJF sulfate concentrations were 0.39 (0.03 - 1.32) and 3.5 (0.7 - 10.9) µg·m^{-3}, respectively. The increased winter [SO_2] was due to emissions from space heating and increased power generation.

Sulfate concentrations were also lower in summer than winter (**Figure 9(f)**, **Figure 11(b)**, **Figure 11(d)**). The mean SO_2 to sulfate ratio was nearly 1:16 in summer vs. 1:8 in winter despite gas-to-particle conversion increases with decreasing temperature (**Figure 2(a)**, **Figure 11(d)**). Gas-to-particle conversions take time, for which sulfate concentrations showed a lower increase than [SO_2]. Since SO_2 emissions and gas-to-particle conversion are lower in summer than winter (**Figure 11(d)**), the high summer ratio suggests that some sulfate stems from advection as sulfate aerosols form during transport [14] [37]. WRF/Chem simulations showed that in the Interior, under typical winter conditions, notable sulfate aerosol concentrations occurred about 100 km or so from the SO_2-emission sources [14].

Available sulfate, wind direction and SO_2 data overlapped for 8/19/2011 to 12/31/2014 (cf. **Table A2**). Daily means of sulfate and maximum [SO_2] correlated 44.3% (R = 0.666) (**Table 3**). Both sulfate and [SO_2] also showed marginal, but significant correlation with wind direction (**Table B3**). Even stronger relations between [$PM_{2.5}$], sulfate and wind direction were found for the North Pole and Peger Rd winter speciation data (**Figure 12(a)**). As aforementioned, [$PM_{2.5}$] went up when wind blew from certain sectors (**Figure 9(e)**). These findings also hint at [SO_2] sources in the far-field. Note that the downtown site might be affected by sulfate emissions from the coal-burning downtown power plant, which would explain the enhanced variability as compared to the other sites (**Figure 12(a)**).

(a)

(b)

(c)

(d)

(e)

(f)
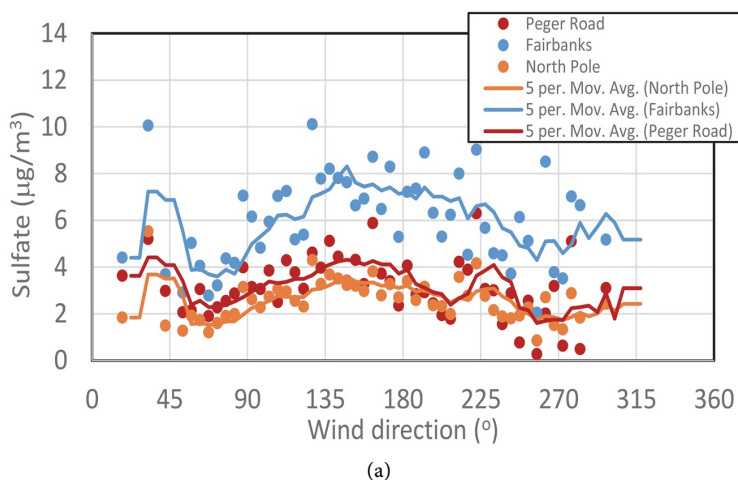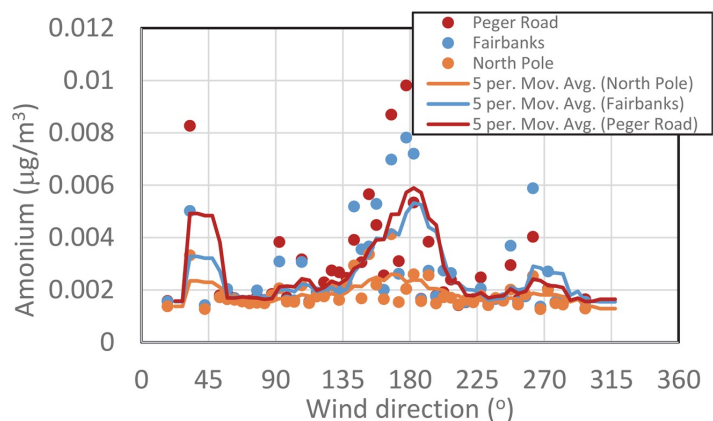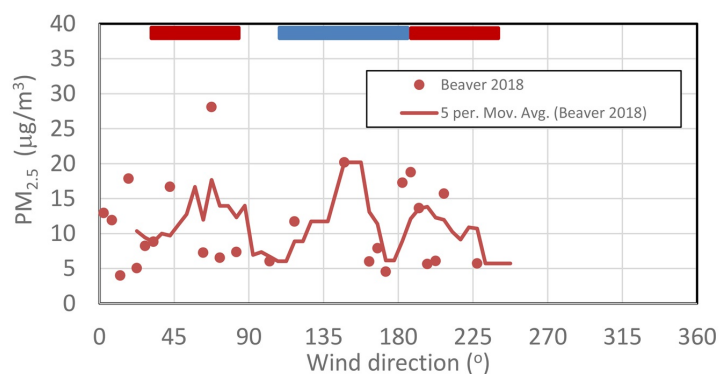
Figure 12. 5˚-sector mean concentrations of (a) sulfate, (b) ammonium vs. wind direction as observed in 2008/09 at three sites in the FMA in the 2008/09 cold season. September to April 5˚-sector mean [PM$_{2.5}$] vs. wind direction at the villages of (c) Beaver, (d) Chalkyitsik, (e) Circle and (f) Ft. Yukon. See **Figure 1** for locations. Wind direction sectors marked with red and blue bars indicate wind direction sectors for which the sites are in the downwind of the village and hotsprings, respectively.
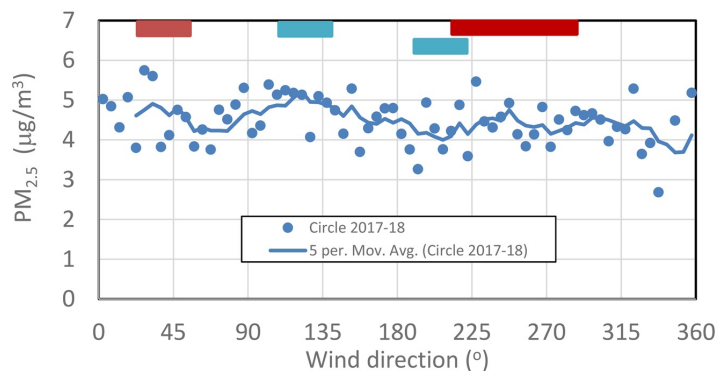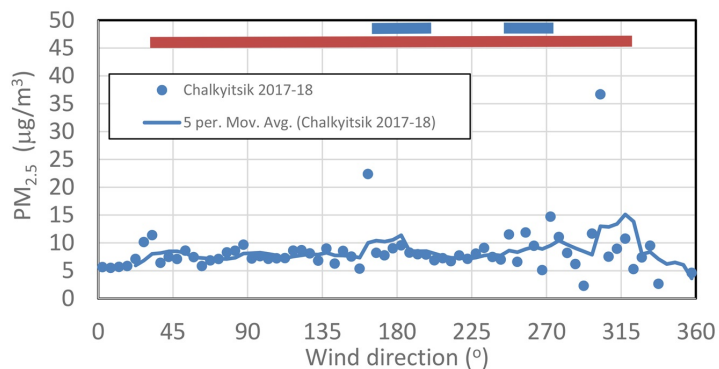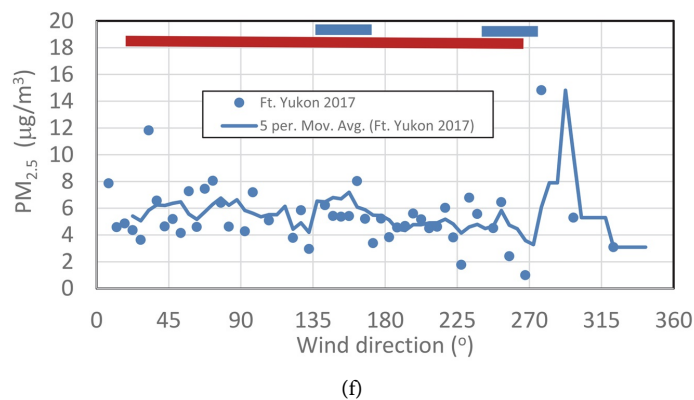
Sulfate correlated less with its precursor SO$_2$ than with ammonium (**Table 3**). The high positive correlation between sulfate and ammonium suggests a common source. Fires emit PM$_{2.5}$ and its precursor gases NO$_2$, VOC, and NH$_3$ as well as small amounts of SO$_2$. However, in the FMA, observed [NH$_3$] were typically lower than sulfate concentrations in both summer and winter (cf. **Figure 8(g)**, **Figure 11(b)**). Furthermore, in 2005 to 2014 (period of speciation data), wildfires burned in different directions from the FMA (cf. also **Figure 4**). Thus, emissions from wildfires fail to explain the distinct preference for elevated concentrations for specific wind sectors. Since the fire season is May thru September, wildfires also fail to explain the winter correlations (**Figure 10(a)**).

In the cold season 2008/09, wind direction and sulfate showed low, but significant correlation at the Fairbanks (R = 0.142), North Pole (R = 0.058) and Peger Rd (R = −0.103) sites (cf. **Figure 8(g)**, **Figure 11(a)**). The different signs are due to local primary emissions dominating the PM$_{2.5}$ composition. Using only data for wind directions of elevated concentrations (defined here as mean plus one standard deviation) yielded R = −0.193, R = −0.185, R = −0.167 for wind directions and sulfate (all significant at >95% confidence). Correlations between these wind directions and elevated ammonium were smaller than for sulfate, but significant as well.

The correlation of sulfate concentrations observed for these directions at different sites were R = 0.890, R = 0.873 and R = 0.764 for the Fairbanks vs. North Pole, North Pole vs. Peger Rd, and Peger Rd vs. Fairbanks sites (at 95%, 90% and 90% confidence), respectively. Correlation coefficients for ammonium were R = 0.759, R = 0.699 (both significant), and R = 0.772 (non-significant) for these pairs of sites. For correlations of other species among these three sites during the 2008/09 cold season see **Table B4**.

Ozone concentrations showed distinct differences with wind direction for both the warm and cold season (**Figure 9(e)**). In the ENE to W sectors, cold

season [O_3] was much lower than in the other sectors. This finding hints at an O_3-sink for these directions. In the warm season, the long daylight accelerates photolysis. Biogenic VOC emissions from the boreal forest and soils as well as wildfires may contribute to O_3 formation. The stronger mixing during the warm than cold season also may contribute to the difference seen between these seasons.

There are 10 hot springs within less than 180 km of Fairbanks in the WNW and ENE to ESE sectors (Figure 1). Besides minerals these geothermal sites hold sulfate and ammonia; the 1912, 1917, 1972 and 1992 analyses of the healing water at Chena Hot Springs, for instance, indicated 89, 78, 68, and 56.1 ppm sulfate dissolved in water, respectively; in 1972, 2.7 ppm ammonia dissolved in the healing water were reported [50].

Only few studies on gases emanating from hot springs exist. Gas samples collected at hot springs in Yellowstone Park never contained detectable amounts of SO_2, but all contained H_2S [51]. This finding is consistent with the higher water solubility and lower pK of SO_2 than H_2S (1.9 vs. 6.88). Many gas samples also contained notable amounts of NH_3 [52].

In the atmosphere, H_2S oxidizes to SO_2 [51]. According to thermodynamic results, reaction of H_2S with O_3 produces $SO_2 + H_2O$ with the lowest value of Gibbs energy ($\Delta G° = -645.84$ kJmol^{-1}) aka free enthalpy [43]. Cold season [O_3] was on average lower when winds came from the directions of hot springs (Figure 9(g)). In the warm season, biogenic emissions yield large amounts of VOC, which also reacts with O_3. Furthermore, NO from photolysis affects [O_3]. These differences in potential reaction paths can explain the quite different behavior of O_3 as a function of wind direction.

In the 2005-2014 speciation climatology (Figure 8(f)), nitrate and ammonium as well sulfate and ammonium correlated nearly 60% (R = 0.772) and 84% (R = 0.914), respectively (Table 2). Ammonium and sulfate correlated with non-metals nearly 89% (R = 0.941) and 92% (R = 0.957). Hot springs are known to degas bromine and selenium—both are non-metals.

Unfortunately, at none of the known Interior hot-springs, gas measurements were performed. However, at Chena, Manley, Tolovana and Hutlinana Hot Springs slight H_2S odor has been observed.

We analyzed the [$PM_{2.5}$] collected in the Yukon Flats for September 2017 to April 2018 [34]. The sites at Beaver (population of 84) and Circle (population of 104) are close to the Dall and Circle Hot Springs (Figure 1). At Beaver, slightly elevated [$PM_{2.5}$] occurred for winds from the 45° to 60° and 130° to 225° sectors (Figure 12(c)). The sector between about 130° and 180° is downwind of hot springs, while the other sectors with elevated [$PM_{2.5}$] are due to the village. At Circle, elevated [$PM_{2.5}$] were observed for the sectors around 200° and 130° that correspond to the major directions of downwind hot springs (compare Figure 1, Figure 12(d)). Despite Chalkyitsik (population of 69) and Ft. Yukon (population of 583) are farther away from hot springs than Circle and Beaver, [$PM_{2.5}$] were slightly elevated when the winds blew from the directions of hot springs

(Figure 12(e) and Figure 12(f)). The peak at around 270° for Ft. Yukon was related to the airport where huge cargo planes and small aircrafts of several airlines take off/land once a week and daily, respectively. In September, the Canadian border fire still burned and caused the peak in $[PM_{2.5}]$ around 300° observed at Chalkyitsik [34].

Based on 1) the similar water composition of the Interior and some Yellowstone hot springs, 2) the presence of H_2S at Interior hot springs, 3) the findings at the sites of the Tribal Air Quality Network in the Yukon Flats, and the fact that when the FMA was in the downwind of hot springs 4) elevated sulfate and ammonium concentrations and 5) elevated $[PM_{2.5}]$ occurred at all sites in the FMA concurrently (Figure 9(c), Figure 12(a) and Figure 12(b), 6) the high correlation between ammonium, sulfate and non-metals (Table 3), 7) the twice as high SO_2 to sulfate ratio in summer when $[O_3]$ are up, than in winter when $[O_3]$ are low (Figure 11), 8) the moderate, negative, but significant correlation between sulfate and ozone (Table 3), and 9) the reduced $[O_3]$ in the wind-direction sectors where sulfate concentrations were elevated (Figure 11(e)), as well as 10) the results from WRF/Chem studies [14], one may assume that some of the sulfate and ammonium aerosols might have geothermal origin.

3.6. Short-Time Scale: Examples of Typical Winter Weather Conditions

The cases of late January into February 2008 and late December 2008 into January 2009 are examples of the fate of $[PM_{2.5}]$ during several days of extremely cold weather (Figure 13). The low near-surface temperatures boosted heating and increased emissions. The calm wind (not shown) meant low ventilation and the temperature inversions strengthened (Figure 13(a) and Figure 13(b)). The inversions capped the near-surface air layers and hindered the exchange of polluted air with less polluted air aloft. Gaseous and particulate matter accumulated in the stagnant air (Figure 13(c) and Figure 13(d)). According to the radiosonde soundings (Figure 13(b)), a light destabilization of the near-surface layer started in the afternoon of January 1 (Alaska Standard Time) and persisted, at least, for 24 hours. During this time, $[PM_{2.5}]$ decreased below the NAAQS (Figure 13(d)). Then the wind calmed down and slightly took up after January 6 before calming down again. Similar happened in the other case; wind was calm until February 9, increased for about a day and was calm again (Figure 13(a)). Snowfall occurred on February 18 to 22, 2008 and on January 14 to 16, 2009. In both cases, the snow event reduced the $[PM_{2.5}]$ (Figure 13(c) and Figure 13(d)).

Subsidence inversions frequently occur in the Interior [33]. On the contrary to the two cases discussed above, they are governed by the synoptic scale. Table 4 illustrates an example of the retrieval of multi-layered temperature inversions [53] based on the thermodynamic sounding station at Fairbanks International Airport for 9-28 to 9-29-2018 and 10-1 to 10-2-2018. The sinking air mass (e.g., adiabatic compression) initiated the formation of an anti-cyclone elevated inversion. The multiple discernible elevated temperature-inversion layers illustrate

the complex vertical structure (Table 4). Continued sinking reduced the volume underneath the inversion, for which the aerosol content increased. Daily mean [PM$_{2.5}$] (with respect to Alaska Standard time AST=UTC-8h) were 4.3, 6.0, 6.6, and 9.8 μg·m^{-3} on September 28, 29, and October 2 and 3, respectively. No concentration and radio-soundings data were available for September 30, October 1, 2018 and September 30 0000 UTC and 1200 UTC, respectively. Concurrently, emissions accumulated under the temperature inversion. Note that in the FMA, the mean, maximum and median effective emissions heights of point sources are 155.75 m, 18.59 m and 25.49 m, respectively. Most residences are two story buildings.

Table 4. Temperature inversion heights of surface-based inversions (SBI), the first (EI-1) and second elevated inversion (EI-2) for the 9/28 to 9/29/2018 and 10/1 to 10/2/2018 0000 and 1200 UTC thermodynamic soundings at PAFA. Here -.- indicates non-existing.

Sounding	Inversion heights		
	SBI (m)	EI-1 (m)	EI-2 (m)
2018/09/28 0000 UTC	-.-	1545	2979
2018/09/28 1200 UTC	633	1625	2649
2018/09/29 0000 UTC	-.-	1848	-.-
2018/09/29 1200 UTC	252	1236	1770
2018/10/01 0000 UTC	-.-	709	1354
2018/10/01 1200 UTC	815	1736	2554
2018/10/02 0000 UTC	-.-	1675	3753
2018/10/02 1200 UTC	362	1219	-.-

(a)
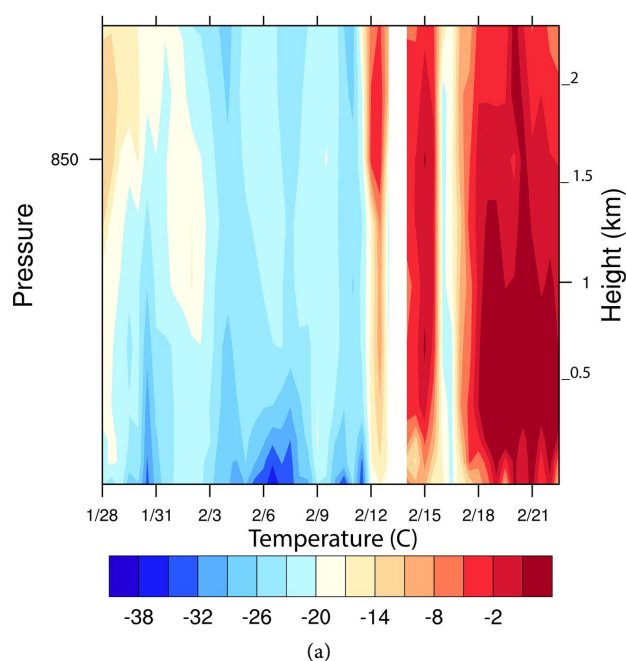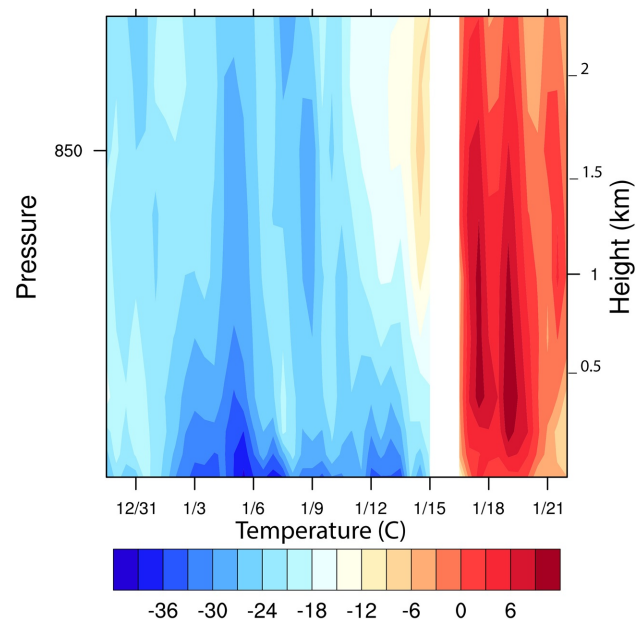
(b)
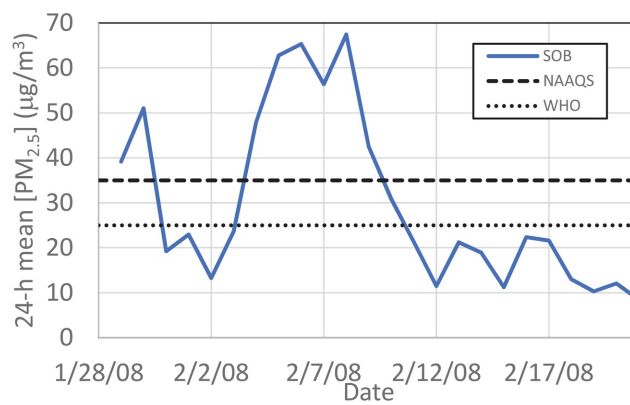
(c)
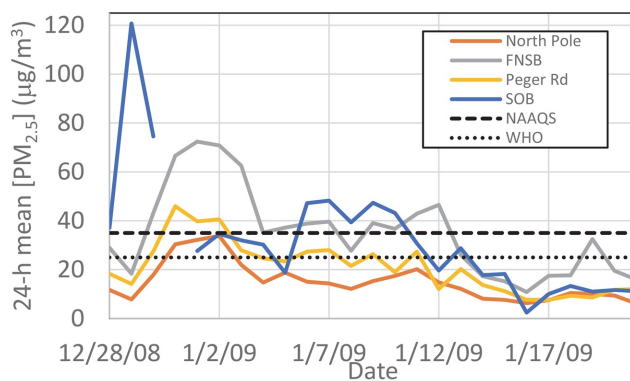
(d)

Figure 13. Temporal evolution of the (a)-(b) thermal structure of the atmospheric boundary layer retrieved by radiosondes launched at PAFA at 0000 and 1200 UTC (2300 and 1100 Alaska standard time) with the lowest values taken from the surface observations, and (c)-(d) observed 24-h mean [PM$_{2.5}$] for (a), (c) 1/28 -2/4/2008, and (b), (d)12/28/2008 to 1/4/2009. White areas in (a) and (b) indicate missing soundings.

4. Impact of Emission Changes on PM$_{2.5}$ Climatology

To compare the changes in concentrations due to meteorology and low frequency variability with those from known emissions changes we determined the trends. In general, these trends are numerical results. Like for the correlations, these trends are given with several digits to see impacts. By no means are these digits an indicator of the measurement accuracy.

We determined changes in [PM$_{2.5}$] caused by altered emissions for comparison with those due to influences from large-scale teleconnections. On average from 1999 to 2018, cold season [PM$_{2.5}$] decreased by 0.1796 µg·m^{-3}·y^{-1} (Table 5).

Commonly, CO serves as a tracer for biomass (*i.e.* also wood) burning [54] due to its relative long lifetime [37]. Daily maximum [CO] decreased about 0.3 ppb·y^{-1} from 1980-2018, 0.3 ppb·y^{-1} from 1980-2009, and 0.03 ppb·y^{-1} from 2011-2018. Between 2005 and 2014, cold season [CO] decreased 94 ppb·y^{-1}. Annual mean [NO$_2$] and [O$_3$] increased about 0.73 ppb·y^{-1} and 0.84 ppb·y^{-1} based on the available data (Table A2).

4.1. Tier 2 Emission Standards for New Vehicles

In the 2005-2014 climatology, PM$_{2.5}$ composition changed at various scales and differed among seasons (e.g. Figure 8). Concentrations of nitrate, sulfate, ammonium, OC, EC, metals, and non-metals decreased by about 0.006, 0.473, 0.380, 4.952, 0.409, 0.155 and 0.152 µg·m^{-3} per decade (Table 5). The overturn of the vehicle fleet to Tier 2 compliance contributed to the gradual overall decrease in sulfate. This decrease was an order of magnitude larger than changes in all other species.

Table 5. Calculated changes of [PM$_{2.5}$] and selected species concentrations during different periods as observed at the Fairbanks State Office Building site.

	Temporal change (µg·m^{-3}·y^{-1})							
	PM$_{2.5}$	Sulfate	Nitrate	Ammonium	OC	EC	Metal	Non-metal
2/1999-3/31/2018	−0.1796	-.-	-.-	.-.	-.-	-.-	-.-	-.-
3/17/2005-12/31/2014	−0.0243	−0.0473	−0.0006	−0.0380	−0.4952	−0.0409	−0.0155	−0.0152
Warm season 2005-2014	−0.1095	−0.0179	−0.0003	−0.0114	−0.5080	−0.0213	−0.0270	−0.0058
Cold season 2005-2014	0.0717	−0.0964	−0.0055	−0.0701	−0.5722	−0.5722	−0.0037	−0.0307
3/17/2005-12/31/2006	0.0003	−0.0026	−0.0032	0.2032	0.2620	0.2780	−0.1802	0.1529
Cold season 2005-2006	0.0751	0.1467	0.1005	0.1512	1.8366	0.2900	0.0060	0.0488
1/1/2007-12/31/2014	−0.0005	−0.0897	−0.0052	−0.0657	−0.6545	−0.0632	−0.0159	−0.0270
Cold season 2007-2014	−0.1527	−0.1611	−0.0241	−0.1117	−0.7626	−0.0965	−0.0080	−0.0148
3/17/2005-5/31/2010	0.0042	−0.0025	−0.0320	0.0875	0.2431	0.0461	0.0003	0.0462
Cold season 2005-2010	1.3017	0.1361	0.0749	0.0978	−0.1304	0.0423	0.0228	0.1294
6/1/2010-12/31/2014	−0.0001	0.0667	0.0225	0.0084	−0.0004	−0.0200	−0.0079	0.0237
Cold season 2010-2014	−0.1076	−0.0393	−0.0027	−0.4760	0.1152	−0.0606	−0.0031	−0.0500

4.2. Low Sulfur Fuel for Rural Areas

The tightened sulfur-fuel standard for rural Alaska coincided with the wood-stove change-out program. Nevertheless, we examined whether an impact of this measure on [PM$_{2.5}$] was observable in the FMA. The number of vehicles using diesel with highway/rural standard while traveling in the FMA was small compared to the local vehicle fleet. Results of WRF/Chem simulations showed that reduced fuel sulfur content would decrease [PM$_{2.5}$] downwind of the FMA with marginal benefits close to the urban emission sources [14]. No measurements existed outside of the FMA at distances where—if at all—differences could be expected according to the WRF/Chem simulations. Based on these facts, we may assume that the impact of low sulfur fuel for rural areas on the urban sulfate aerosol most likely was negligible.

4.3. Boom of Woodstove Additions in 2007

Prior to and after the rapid increase in fuel prices in 2007, cold season [PM$_{2.5}$] increased 0.0717 and decreased 0.1527 µg·m^{-3}·y^{-1}, respectively (Table 5). Prior to 2007, cold season sulfate, OC and CO concentrations increased by 0.1467 µg·m^{-3}·y^{-1}, 1.8366 µg·m^{-3}·y^{-1} and 2.48 ppb·y^{-1}. From 2007 onwards, cold season sulfate, OC and CO concentrations decreased about 0.1661 µg·m^{-3}·y^{-1}, 0.7626 µg·m^{-3}·y^{-1} (Table 5) and 6.7 ppb·y^{-1} (Figure 14). Prior to 2007, cold season [NH$_4$] increased 0.151 µg·m^{-3}·y^{-1}, while they decreased by 0.1117 µg·m^{-3}·y^{-1} thereafter (Table 5).

(a)

(b)

(c)

(d)

(e)

(f)

(g)

(h)
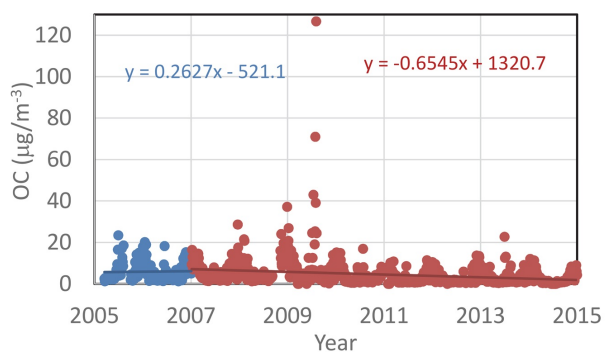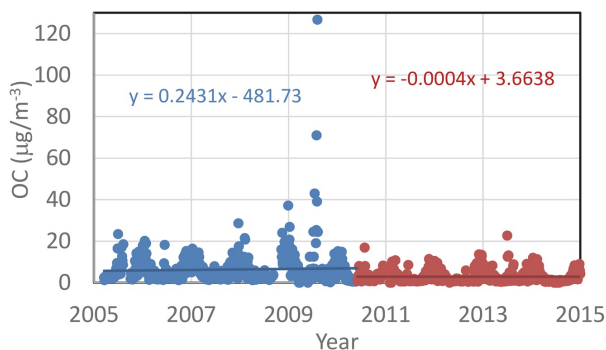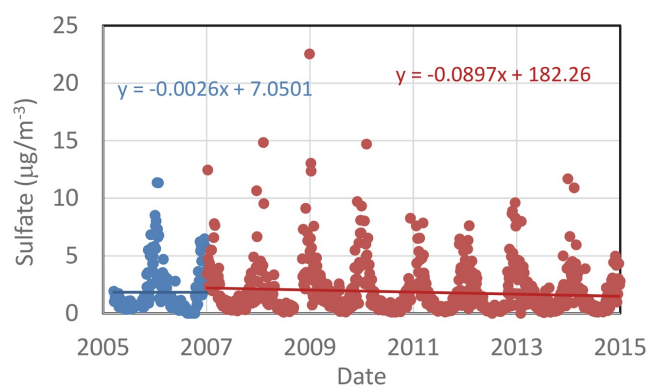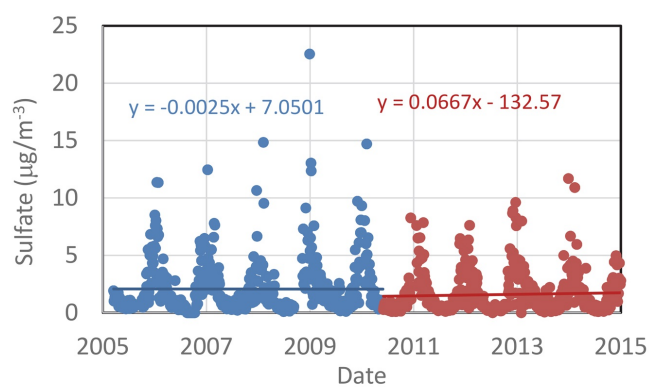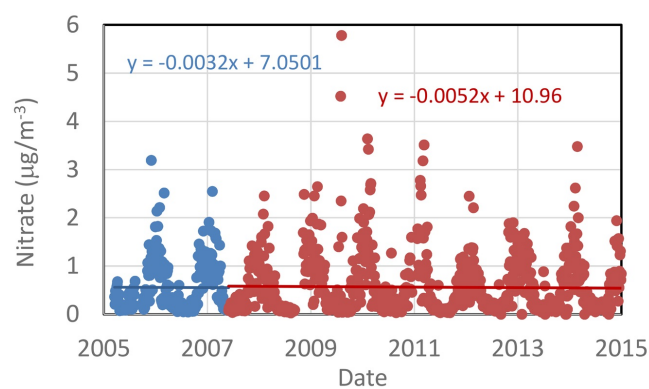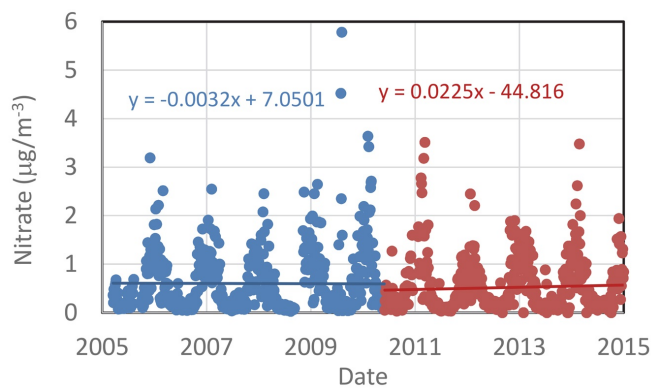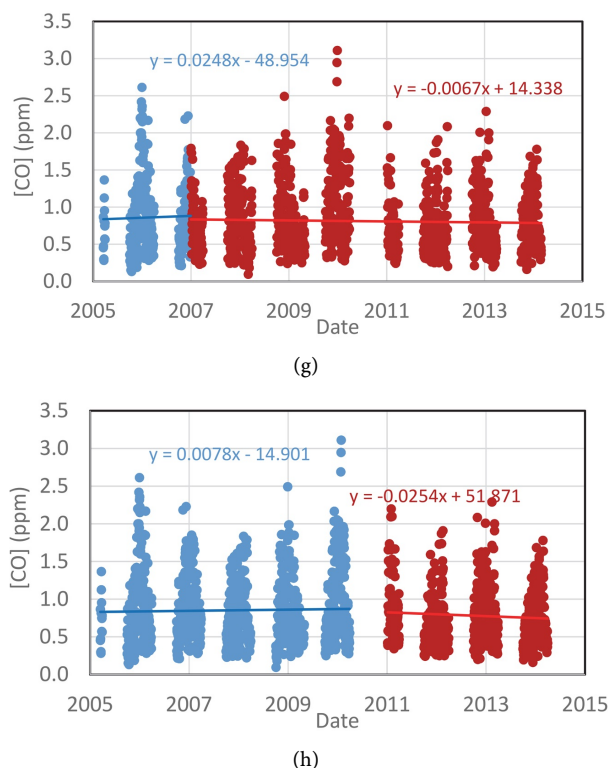
Figure 14. Temporal evolution of species concentrations in response to the 2007 (a), (c), (e), (g) and 2010 (b), (d), (f), (h) emissions changes for (a)-(b) OC, (c)-(d) sulfate, (e)-(f) nitrate, and (g)-(h) CO. The site location for CO measurements changed in 2011.

4.4. Woodstove Change-Out Program

From 1999 to the start of the wood-stove change-out program (June 2010), cold season [$PM_{2.5}$] increased by 0.1412 $\mu g \cdot m^{-3} \cdot y^{-1}$. From 3/17/2005 to 5/31/2010, cold season [$PM_{2.5}$] increased 1.3017 $\mu g \cdot m^{-3} \cdot y^{-1}$. Thereafter, it decreased 0.1076 $\mu g \cdot m^{-3} \cdot y^{-1}$ (Table 5). Prior to cold season 2009/10, sulfate, nitrate, [EC] [NH_4] and [CO] increased and [OC] decreased, while thereafter the opposite was true (cf. Figure 14, Table 5).

5. Discussion, Conclusions and Recommendations

A comprehensive air-quality assessment study with relevant environmental parameters and 12 environmental pollutants was performed to explore relevant atmospheric mechanisms responsible for poor air quality in the Fairbanks Metropolitan area. We separated the various factors influencing $PM_{2.5}$ concentrations, its composition, precursor gases and other co-emitted gases by statistical methods.

This study pointed out the need for 1) NH_3 monitoring, 2) a re-thinking about the determination of compliance/non-compliance in regions known to be affected by teleconnections, and 3) isotopic examination of $PM_{2.5}$, ammonium and sulfate to determine the origin of the [NH_3] and sulfate concentrations that cannot be explained by the anthropogenic emissions. When some of the ammo-

nium and sulfate aerosols is of geothermal origin, their isotopes differ from those of the anthropogenic and/or biogenic sources.

The geographic, topographic, and meteorological conditions are mainly responsible for air quality issues during the cold season in the Fairbanks Metropolitan Area. The overturn of the vehicle fleet since 2004 contributed to an overall decrease in sulfate over time. Changes in the fuel used for heating went along with changes in the emissions of precursor gases and composition of $PM_{2.5}$. Since the species of $PM_{2.5}$ differ in weight, and aerosol formation has affinity for certain chemical reaction paths, changes in the precursor ratios led to changes in total $PM_{2.5}$ weight and hence $[PM_{2.5}]$. All other conditions being the same, shifts in aerosol formation and/or emissions to a greater percentage of sulfates at the cost of nitrate, for instance, increase the $[PM_{2.5}]$. The introduction of Tier 2 vehicles led to an overall decrease of sulfate concentrations and, in turn an overall decrease of $[PM_{2.5}]$ as well. Overall absolute values of changes in $[PM_{2.5}]$ and the concentrations of its species in response to emission changes were of the order $0.1 \ \mu g \cdot m^{-3} \cdot y^{-1}$ except sulfate, and in cold season 2005 and 2006, OC. In conclusion, all responses to emissions changes were lower than the mean changes in annual means caused by low frequency variability associated with teleconnections.

Comparison of the observed concentration changes in response to emissions changes and the observed concentration differences in response to decadal and inter-annual variability suggest that a final assessment of success or failure of emissions-control measures should bear the large-scale atmospheric coupling and variability in mind. This consideration would help establishing a definitive impact on the air-quality prevention measures. On average over all data, cold season $[PM_{2.5}]$ differed $1.8 \ \mu g \cdot m^{-3}$ between years with positive and negative PDO as well as $3.6 \ \mu g \cdot m^{-3}$ between years of positive and negative SOI. These differences are at least one order of magnitude larger than those observed in response to emissions changes. Changes anticipated due to the different emissions-control measures tested in WRF/Chem simulations [14] [15] [16] and the low frequency caused differences in $[PM_{2.5}]$ found in our study were of similar magnitude.

An important finding was that atmospheric teleconnections from changes in the general circulation (here examined exemplarily by the PDO, SOI, and NP) can have significant influence on air quality in the FMA. This new finding contributes to the rational analysis of pollutant regulation. The sudden shift in PDO in 1976, for instance, increased monthly mean temperature up to more than 6 K. Since for temperatures less than 10°C 24-h average $[PM_{2.5}]$ decreased non-linearly with increasing temperature, a regime shift like in 1976 might lead to incorrect assessment of failure/success of an emission-control measure due to the associated sudden change in air temperature. Thus, one may conclude that the current recommendation of 5-years in assessment of compliance might be too short in regions affected by large-scale atmospheric teleconnections.

The EOF analysis indicated that drivers for low air quality differed among

seasons and that DJF air quality is the hardest to predict.

The study also revealed that elevated $PM_{2.5}$, sulfate and ammonium concentrations occurred in the FMA at all sites concurrently when winds blew from the general directions where hot springs are located. Likewise elevated $[PM_{2.5}]$ was found at the four sites in the Yukon Flats when winds blew from the general directions of hot springs.

In the cold season, $[O_3]$ was lower when winds blew from the general directions of hot springs than for other wind directions. Together with the presence of H_2S odor at the hot springs, the high correlation between ammonium, sulfate and non-metals as well as results from the literature, these findings suggest to conclude that some of the observed sulfate and ammonium aerosols might have geothermal origin. Despite the sources have not yet been pin-pointed finally, the finding of elevated $[PM_{2.5}]$ with winds from directions of hot springs may be used to issue preventive emissions-control measures when the respective wind directions are in the forecast.

Under extremely cold weather events like in winter 2009 and 2010, authorities may enforce emissions reductions to an unavoidable minimum. Such a—yet to be determined—minimum must still guarantee unavoidable traffic and the generation of sufficient electricity and heating for the citizens, their pets and livestock to survive. Consequently, appropriate, but, perhaps, massive measures have to be called at the State level prior to exceedance of the NAAQS. Doing so may avoid the accumulation of gaseous and particulate matter in the near-surface layer to unhealthy levels during long-lasting extremely cold weather conditions. Such a measure, for instance, could be a ban on individual traffic. Today numerical weather predictions for a week out are very reliable. Predictions of $[PM_{2.5}]$ using a state-of-the-art model like the WRF/Chem package may serve to assess the needed degree of emissions restrictions to avoid exceedances of the NAAQS. Such activities, of course, require an emergency team of experts in internal medicine, air quality and meteorology well familiar with numerical predictions of $[PM_{2.5}]$, and high-ranking State administrators.

Acknowledgements

Conflicts of Interest

The authors declare no conflicts of interest regarding the publication of this paper.

References

[1] Pope, I.C.A., Dockery, D.W. and Schwartz, J. (1995) Review of Epidemiological Evidence of Health Effects of Particulate Air Pollution. *Inhalation Toxicology*, **7**, 1-18. https://doi.org/10.3109/08958379509014267

[2] Liu, J.C., Pereira, G., Uhl, S.A., Bravo, M.A. and Bell, M.L. (2015) A Systematic Review of the Physical Health Impacts from Non-Occupational Exposure to Wildfire Smoke. *Environmental Research*, **136**, 120-132. https://doi.org/10.1016/j.envres.2014.10.015

[3] Strickland, M.J., Hao, H., Hu, X., Chang, H.H., Darrow, L.A. and Liu, Y. (2015) Pediatric Emergency Visits and Short-Term Changes in $Pm_{2.5}$ Concentrations in the U.S. State of Georgia. *Environmental Health Perspectives*, **124**, 690-696. https://doi.org/10.1289/ehp.1509856

[4] Segersson, D., Eneroth, K., Gidhagen, L., Johansson, C., Omstedt, G., Nylén, A.E., *et al.* (2017) Health Impact of PM_{10}, $PM_{2.5}$ and Black Carbon Exposure Due to Different Source Sectors in Stockholm, Gothenburg and Umea, Sweden. *International Journal of Environmental Research and Public Health*, **14**, 742. https://doi.org/10.3390/ijerph14070742

[5] Sinkemani, R., Sinkemani, A., Li, X. and Chen, R. (2018) Risk of Cardiovascular Disease Associated with the Exposure of Particulate Matter ($PM_{2.5}$): Review. *Journal of Environmental Protection*, **9**, 607-618. https://doi.org/10.4236/jep.2018.96038

[6] EPA (2014) Emissions Inventory Guidance for Implementation of Ozone [and Particulate Matter] National Ambient Air Quality Standards (NAAQS) and Regional Haze Regulations—Draft.

[7] Tran, H.N.Q. and Mölders, N. (2011) Investigations on Meteorological Conditions for Elevated $PM_{2.5}$ in Fairbanks, Alaska. *Atmospheric Research*, **99**, 39-49. https://doi.org/10.1016/j.atmosres.2010.08.028

[8] National Research Council (2002) The Ongoing Challenge of Managing Carbon Monoxide Pollution in Fairbanks, Alaska: Interim Report (2002). Washington DC, 154.

[9] Mölders, N. and Kramm, G. (2010) A Case Study on Wintertime Inversions in Interior Alaska with WRF. *Atmospheric Research*, **95**, 314-332. https://doi.org/10.1016/j.atmosres.2009.06.002

[10] Mölders, N., Tran, H.N.Q., Quinn, P., Sassen, K., Shaw, G.E. and Kramm, G. (2011) Assessment of WRF/Chem to Capture Sub-Arctic Boundary Layer Characteristics During Low Solar Irradiation Using Radiosonde, Sodar, and Station Data. *Atmospheric Pollution Research*, **2**, 283-299. https://doi.org/10.5094/APR.2011.035

[11] Mölders, N. and Kramm, G. (2014) Lectures in Meteorology. Springer, Heidelberg, 591. https://doi.org/10.1007/978-3-319-02144-7

[12] Crippa, M., Guizzardi, D., Muntean, M., Schaaf, E., Dentener, F., van Aardenne, J.A., *et al.* (2018) Gridded Emissions of Air Pollutants for the Period 1970-2012 within EDGAR V4.3.2. *Earth System Science Data Discussion*, **10**, 1987-2013. https://doi.org/10.5194/essd-2018-31

[13] Scientific Community (2014) WRF/Chem User Guide Version 3.6. NOAA-ESSL, Boulder, 75.

[14] Mölders, N. (2013) Investigations on the Impact of Single Direct and Indirect, and Multiple Emission-Control Measures on Cold-Season Near-Surface $PM_{2.5}$ Concentrations in Fairbanks, Alaska. *Atmospheric Pollution Research*, **4**, 87-100. https://doi.org/10.5094/APR.2013.009

[15] Tran, H.N.Q. and Mölders, N. (2012) Wood-Burning Device Changeout: Modeling the Impact on $PM_{2.5}$ Concentrations in a Remote Subarctic Urban Nonattainment Area. *Advances in Meteorology*, **2012**, Article ID: 853405. https://doi.org/10.1155/2012/853405

[16] Tran, H.N.Q. and Mölders, N. (2012) Numerical Investigations on the Contribution of Point Source Emissions to the $PM_{2.5}$ Concentrations in Fairbanks, Alaska. *Air Pollution Research*, **3**, 199-210. https://doi.org/10.5094/APR.2012.022

[17] Samet, J.M., Dominici, F., Curriero, F.C., Coursac, I. and Zeger, S.L. (2000) Fine Particulate Air Pollution and Mortality in 20 US Cities, 1987-1994. *New England Journal of Medicine*, **343**, 1742-1749. https://doi.org/10.1056/NEJM200012143432401

[18] Dominici, F., Peng, R.D., Bell, M.L., Pham, L., McDermott, A., Zeger, S.L., *et al.* (2006) Fine Particulate Air Pollution and Hospital Admission for Cardiovascular and Respiratory Diseases. *Journal of the American Medical Association*, **295**, 1127-1134. https://doi.org/10.1001/jama.295.10.1127

[19] Jerrett, M., Burnett, R.T., Pope III, C.A., Ito, K., Thurston, G., Krewski, D., *et al.* (2009) Long-Term Ozone Exposure and Mortality. *New England Journal of Medicine*, **360**, 1085-1095. https://doi.org/10.1056/NEJMoa0803894

[20] Calef, M.P., Varvak, A., McGuire, A.D., III, F.S.C. and Reinhold, K.B. (2015) Recent Changes in Annual Area Burned in Interior Alaska: The Impact of Fire Management. *Earth Interactions*, **19**, 1-17. https://doi.org/10.1175/EI-D-14-0025.1

[21] Randerson, J.T., van der Werf, G.R., Giglio, L., Collatz, G.J. and Kasibhatla, P.S. (2018) Global Fire Emissions Database, Version 4.1 (GFEDv4). ORNL DAAC, Oak Ridge.

[22] Shulski, M. and Wendler, G. (2007) The Climate of Alaska. University of Alaska Press, Fairbanks, 216.

[23] Trenberth, K.E. and Hurrell, J.W. (1994) Decadal Atmosphere-Ocean Variations in the Pacific. *Climate Dynamics*, **9**, 303-319. https://doi.org/10.1007/BF00204745

[24] Ropelewski, C.F. and Jones, P.D. (1987) An Extension of the Tahiti-Darwin Southern Oscillation Index. *Monthly Weather Review*, **115**, 2161-2165. https://doi.org/10.1175/1520-0493(1987)115<2161:AEOTTS>2.0.CO;2

[25] Zhang, Y., Wallace, J.M. and Battisti, D.S. (1997) ENSO-Like Interdecadal Variability: 1900-93. *Journal of Climate*, **10**, 1004-1020. https://doi.org/10.1175/1520-0442(1997)010<1004:ELIV>2.0.CO;2

[26] Mantua, N.J., Hare, S.R., Zhang, Y., Wallace, J.M. and Francis, R.C. (1997) A Pacific Interdecadal Climate Oscillation with Impacts on Salmon Production. *Bulletin of the American Meteorological Society*, **78**, 1069-1079. https://doi.org/10.1175/1520-0477(1997)078<1069:APICOW>2.0.CO;2

[27] Kim, J., Waliser, D.E., Mattmann, C.A., Mearns, L.O., Goodale, C.E., Hart, A.F., *et al.* (2013) Evaluation of the Surface Climatology over the Conterminous United States in the North American Regional Climate Change Assessment Program Hindcast Experiment Using a Regional Climate Model Evaluation System. *Journal of Climate*, **26**, 5698-5715. https://doi.org/10.1175/JCLI-D-12-00452.1

[28] Mölders, N., Bruyère, C.L., Gende, S. and Pirhalla, M.A. (2014) Assessment of the 2006-2012 Climatological Fields and Mesoscale Features from Regional Downscaling of CESM Data by WRF-Chem over Southeast Alaska. *Atmospheric and Climate Sciences*, **4**, 589-613. https://doi.org/10.4236/acs.2014.44053

[29] von Storch, H. and Zwiers, F.W. (1999) Statistical Analysis in Climate Research. Cambridge University Press, Cambridge, 484 p.

https://doi.org/10.1017/CBO9780511612336

[30] Scientific Community (2019) The NCAR Command Language (Version 6.6.2) [Software]. UCAR/NCAR/CISL/TDD, Boulder.

[31] Madden, J.M., Mölders, N. and Sassen, K. (2015) Assessment of WRF/Chem Simulated Vertical Distributions of Particulate Matter from the 2009 Minto Flats South Wildfire in Interior Alaska by CALIPSO Total Backscatter and Depolarization Measurements. *Open Journal of Air Pollution*, **4**, 119-138. https://doi.org/10.4236/ojap.2015.43012

[32] Bourne, S.M., Bhatt, U.S., Zhang, J. and Thoman, R. (2010) Surface-Based Temperature Inversions in Alaska from a Climate Perspective. *Atmospheric Research*, **95**, 353-366. https://doi.org/10.1016/j.atmosres.2009.09.013

[33] Mayfield, J.A. and Fochesatto, J. (2013) The Layered Structure of the Winter Atmospheric Boundary Layer in the Interior of Alaska. *Journal of Applied Meteorology and Climatology*, **52**, 953-973. https://doi.org/10.1175/JAMC-D-12-01.1

[34] Edwin, S.G. and Mölders, N. (2018) Particulate Matter Exposure of Rural Interior Communities as Observed by the First Tribal Air Quality Network in the Yukon Flats. *Journal of Environmental Pollution*, **9**, 1425-1448. https://doi.org/10.4236/jep.2018.913088

[35] World Health Organization (2006) WHO Air Quality Guidelines for Particulate Matter, Ozone, Nitrogen Dioxide and Sulfur Dioxide. Summary of Risk Assessment, World Health Organization, Geneva, 22.

[36] EPA (2011) National Ambient Air Quality Standards (NAAQS). https://www.epa.gov/environmental-topics/air-topics

[37] Seinfeld, J.H. and Pandis, S.N. (1997) Atmospheric Chemistry and Physics, from Air Pollution to Climate Change. John Wiley & Sons, Hoboken.

[38] Hartmann, B. and Wendler, G. (2005) The Significance of the 1976 Pacific Climate Shift in the Climatology of Alaska. *Journal of Climate*, **18**, 4824-4839. https://doi.org/10.1175/JCLI3532.1

[39] Kramm, G. and Dlugi, R. (1994) Modelling of the Vertical Fluxes of Nitric Acid, Ammonia, and Ammonium Nitrate in the Atmospheric Surface Layer. *Journal of Atmospheric Chemistry*, **18**, 319-357. https://doi.org/10.1007/BF00712450

[40] Tetzlaff, G., Dlugi, R., Friedrich, K., Gross, G., Hinneburg, D., Pahl, U., *et al.* (2002) On Modeling Dry Deposition of Long-Lived and Chemically Reactive Species over Heterogeneous Terrain. *Journal of Atmospheric Chemistry*, **42**, 123-155. https://doi.org/10.1023/A:1015740203204

[41] Lu, Z. and Sokolik, I. (2018) The Impacts of Smoke Emitted from Boreal Forest Wildfires on the High Latitude Radiative Energy Budget—A Case Study of the 2002 Yakutsk Wildfires. *Atmosphere*, **9**, 410. https://doi.org/10.3390/atmos9100410

[42] Kramm, G. and Meixner, F.X. (2000) On the Dispersion of Trace Species in the Atmospheric Boundary Layer: A Re-Formulation of the Governing Equations for the Turbulent Flow of the Compressible Atmosphere. *Tellus*, **52A**, 500-522. https://doi.org/10.1034/j.1600-0870.2000.00984.x

[43] Vahedpour, M., Baghary, R. and Khalili, F. (2013) Prediction of Mechanism and Thermochemical Properties of O_3 + H_2S Atmospheric Reaction. *Journal of Chemistry*, **2013**, Article ID: 659682. https://doi.org/10.1155/2013/659682

[44] Mölders, N., Tran, H.N.Q., Cahill, C.F., Leelasakultum, K. and Tran, T.T. (2012) Assessment of WRF/Chem $PM_{2.5}$ Forecasts Using Mobile and Fixed Location Data from the Fairbanks, Alaska Winter 2008/09 Field Campaign. *Air Pollution Re-*

search, **3**, 180-191. https://doi.org/10.5094/APR.2012.018

[45] Tran, H.N.Q. (2012) Analysis of Model and Observation Data for the Development of a Public PM$_{2.5}$ Air-Quality Advisories Tool (AQUAT). PhD Thesis, Department of Atmospheric Sciences, University of Alaska Fairbanks, Fairbanks, 309.

[46] Magee, N., Curtis, J. and Wendler, G. (1999) The Urban Heat Island Effect at Fairbanks, Alaska. *Theoretical and Applied Climatology*, **64**, 39-47. https://doi.org/10.1007/s007040050109

[47] Mölders, N. and Kramm, G. (2018) Climatology of Air Quality in Arctic Cities—Inventory and Assessment. *Open Journal of Air Pollution*, **7**, 48-93. https://doi.org/10.4236/ojap.2018.71004

[48] Karlsson, P.E., Ferm, M., Tømmervik, H., Hole, L.R., Pihl Karlsson, G., Ruoho-Airola, T., *et al*. (2013) Biomass Burning in Eastern Europe during Spring 2006 Caused High Deposition of Ammonium in Northern Fennoscandia. *Environmental Pollution*, **176**, 71-79. https://doi.org/10.1016/j.envpol.2012.12.006

[49] Sutton, M.A., Place, C.J., Eager, M., Fowler, D. and Smith, R.I. (1995) Assessment of the Magnitude of Ammonia Emissions in the United Kingdom. *Atmospheric Environment*, **29**, 1393-1411. https://doi.org/10.1016/1352-2310(95)00035-W

[50] Chena Hotsprings (2018) Healing Waters. https://chenahotsprings.com/healingwater

[51] Zinder, S. and Brock, T.D. (1977) Sulfur Dioxide in Geothermal Waters and Gases. *Geochimica et Cosmochimica Acta*, **41**, 73-79. https://doi.org/10.1016/0016-7037(77)90187-9

[52] Werner, C., Hurwitz, S., Evans, W.C., Lowenstern, J.B., Bergfeld, D., Heasler, H., *et al*. (2008) Volatile Emissions and Gas Geochemistry of Hot Spring Basin, Yellowstone National Park, USA. *Journal of Volcanology and Geothermal Research*, **178**, 751-762. https://doi.org/10.1016/j.jvolgeores.2008.09.016

[53] Fochesatto, G.J. (2015) Methodology for Determining Multilayered Temperature Inversions. *Atmospheric Measurement Technics*, **8**, 2051-2060. https://doi.org/10.5194/amt-8-2051-2015

[54] Fisher, J.A., Jacob, D.J., Purdy, M.T., Kopacz, M., Le Sager, P., Carouge, C., *et al*. (2010) Source Attribution and Interannual Variability of Arctic Pollution in Spring Constrained by Aircraft (ARCTAS, ARCPAC) and Satellite (AIRS) Observations of Carbon Monoxide. *Atmospheric Chemistry and Physics*, **10**, 977-996. https://doi.org/10.5194/acp-10-977-2010

[55] Ruairuen, W., Fochesatto, G.J., Sparrow, E.B., Schnabel, W., Zhang, M. and Kim, Y.J. (2015) Evapotranspiration Cycles in a High Latitude Agroecosystem: Potential Warming Role. *PLoS ONE*, **10**, e0137209. https://doi.org/10.1371/journal.pone.0137209

Appendix A: Data Availability and Sources

Radiosonde data were obtained from the NOAA ftp site. Monthly mean near-surface temperatures at the Fairbanks International Airport (PAFA) between 1930 and March 2018 stem from the Alaska Climate Research Center. The 1981-2010 climatology of minimum, maximum, and mean temperature, mean wind speed, monthly mean snowfall and precipitation stem from the National Climatic Data Center. Data of the Pacific Decadal Oscillation were taken from http://research.jisao.washington.edu/pdo/PDO.latest [25] [26]. Data of the Southern Oscillation Index stem from the Climate Research Unit [24]. Data of the North Pacific index were downloaded at https://climatedataguide.ucar.edu/climate-data/north-pacific-np-index-trenberth-and-hurrell-monthly-and-winter [23].

Daily total solar radiation, mean 10-m wind speed, gust wind speed, wind direction, mean, maximum and minimum 2-m air temperatures, fuel temperatures and relative humidity, daily mean pressure and accumulated precipitation for Fairbanks from the Bureau of Land Management (BLM) Fairbanks site were downloaded from the Western Region Climate Center. The 2013-lysimeter measurements at the UAF experimental farm that provided soil-volumetric water content of the same soil, but covered with different vegetation, stem from [55].

Data of anthropogenic and fire $PM_{2.5}$ emissions were downloaded from the Emission Database for Global Atmospheric Research [12] and the Global Fire Emissions Database [21] websites respectively. Table A1 lists further information on the data.

If not mentioned otherwise, FMA air-quality data were retrieved from the US EPA. Air-quality data from the Yukon Flats are courtesy to the Council of Athabascan Tribes Governments, Tribes of Beaver, Chalkyitsik, Circle, and Ft. Yukon. See Table A2 for further information on the data.

Table A1. Emission data used in this study.

Dataset	Data information			
	Quantity	Period	Source	Reference
Global Fire Emissions Database v4.1	Monthly/daily $PM_{2.5}$ emissions	1999-2017	https://www.globalfiredata.org/	[21]
Emission Database for Global Atmospheric Research v4.3.2	Fossil and biogenic annual mean $PM_{2.5}$ emissions	1999-2012	http://edgar.jrc.ec.europa.eu/	[12]

Table A2. Chemical species data used in this study. Here AC, RD, WRES, UAF, WCS, FMB, CPR, HR, BR, WS, BR, NP, HA, SOB, CS, PR are the Artisan Courtyard, Riverboat Discovery, Wood River Elementary School, UAF Experimental Farm, Watershed Charter School, Fairbanks North Star Borough Maintenance Building, Chena Pump Rd, Hurst Rd, Water Stillmeyer, Badger Rd, Newby Park, Hamilton Acres, State Office Building, North Pole Christian School and Pioneer Rd sites. North Pole is a city in the FMA. Note that time series may be 1-in-3-days, daily, and may have missing data. Here only the full lengths of IOP are listed. The value in brackets is the number of valid observations.

Data	Data information		
	Site	Period (sample size)	Source
24-h-means of $PM_{2.5}$ concentrations	CPR	1/13-2/16/2016 (38)	
	AC	1/7-3/31/2016 (85)	
	RD	3/1-12/31/2013 (271)	
	WRES	3/29-4/9/2009, 10/12/2010-3/31/2011 (172)	Environmental Protection Agency
	UAF	1/25-3/13/2009 (24)	https://aqs.epa.gov/aqsweb/airdata/download_files.html
	HR	1/1/2013-12/31/2017 (1833)	
	NP	10/15/2013-2/12/2-14 (121)	
	HA	10/1-12/31/2014 (83)	

Continued

	SOB	2/18/1999-3/31/2018 (2511)	
	PR	11/6/2009-5/20/2017 (2686)	
	BR	1/1/2013-4/2/2014, 2/8/2016-3/31/2016 (317)	
	WS	10/1/2014-3/31/2015 (182)	
	WCS	11/13/2009-1/31/2010, 1/18-3/1/2013, 1/1-2/28-2014, 10/1-12/31/2015 (211)	
	CS	2/13/2014-3/31/2014 (35)	
	FMB	2/17-4/1/2010 (33)	
NO$_2$	NCORE	7/1/2014-3/31/2018 (1269)	Environmental Protection Agency https://aqs.epa.gov/aqsweb/airdata/download_files.html
SO$_2$	NCORE	8/19/2011-3/31/2018 (2356)	Environmental Protection Agency https://aqs.epa.gov/aqsweb/airdata/download_files.html
O$_3$	NCORE	8/5/2011-3/31/2018 (2158)	Environmental Protection Agency https://aqs.epa.gov/aqsweb/airdata/download_files.html
CO	NCORE	1/11/1980-5/1/2009, 8/5/2011-3/31/2018 (7602)	Environmental Protection Agency https://aqs.epa.gov/aqsweb/airdata/download_files.html
Speciation	Fairbanks	3/17/2005-12/31/2014	Fairbanks North Star Borough Air Quality Division
	Peger Rd	10/1/2008-3/31/2009, 11/3/2009-3/15/2010, 1/9/2011-2/5/2011	
	North Pole	10/1/2008-3/31/2009	
5-min PM$_{2.5}$	Beaver	9/1/2017-4/30/2018	Council of Athabascan Tribal Governments
	Chalkyitsik	9/1/2017-4/30/2018	
	Circle	9/1/2017-4/30/2018	
	Ft. Yukon	9/1/2017-12/31/2017	

Appendix B: Species-Meteorology Relations

Table B1. Correlation of low frequency variations expressed by PDO, SOI and NP with monthly mean [PM$_{2.5}$]. Significant correlations at 95% or higher confidence according to a paired two-tailed t-test are in bold. Values in brackets are the number of pairs, #, used in the calculations.

	Correlation between [PM$_{2.5}$] and low frequency variation		
	PDO (#)	SOI (#)	NP (#)
2/18/1999-3/31/2018	**0.078** (228)	**−0.069** (228)	**−0.249** (228)
Warm season	**0.131** (76)	**−0.229** (76)	**−0.136** (76)
Cold season	**0.175** (116)	**0.107** (116)	**−0.439** (116)

Table B2. Annual, cold and warm season mean [PM$_{2.5}$] for 2/1999 to 3/2018 under annual, cold and warm season positive or negative means of PDO and SOI as well as under annual, cold and warm season NP lower and higher than the thresholds a, cs, and ws, respectively. Here a = 1012 hPa, cs = 1010 hPa, ws = 1016 hPa are the threshold values for the annual, cold season and warm season.

Index	[PM$_{2.5}$]		
	Annual mean (µg·m^{-3})	Cold season mean (µg·m^{-3})	Warm season mean
PDO positive	10.5	18.2	7.1
PDO negative	14.6	16.4	15.1
SOI positive	11.2	17.4	5.3
SOI negative	14.8	17.1	14.5
NP < a, cs, ws	17.0	17.3	16.3
NP > a, cs, ws	11.5	17.1	5.1

Table B3. Correlation of species for the cold season 2008/09 among the three sites for which speciation data were available. Correlations being significant at 95% confidence or higher according to a two-tailed paired t-test are in bold. Values in brackets give the number of pairs, #, included in the calculations.

	Species correlation coefficient (# of pairs)					
	PM$_{2.5}$	SO$_4$	NO$_3$	NH$_4$	EC	OC
Peger Rd vs. Fairbanks	**0.650** (182)	**0.651** (182)	**0.757** (176)	0.862 (182)	**0.653** (182)	**0.653** (182)
Fairbanks vs. North Pole	**0.914** (182)	**0.914** (182)	**0.861** (177)	**0.821** (182)	**0.915** (182)	**0.915** (182)
North Pole vs. Peger Rd	**0.823** (182)	**0.823** (182)	**0.809** (180)	**0.810** (182)	**0.823** (132)	**0.823** (182)

Table B4. Correlations of speciation concentrations and aerosol precursor-gas concentrations with daily accumulated radiation $R_s\downarrow$, daily mean T, maximum T_{max} and minimum T_{min} air temperatures, daily mean, maximum and minimum fuel temperatures T_{fuel}, $T_{fuel,max}$, $T_{fuel,min}$, as well as daily mean, maxiumum and minimum relative humidity RH, RH_{max}, RH_{min}, mean wind speed, v, wind gusts, v_{gust} and wind direction, dir as observed at the BLM site. Bold values indicate significant correlation at 95% confidence or higher according to a two-tailed paired t-test. Note that correlations represent different observation periods (see **Table A2** for times of data availability). The symbol -.- means no overlapping time of measurements. Cold and warm season refer to October to March and May to August, respectively.

Quantity	PM$_{2.5}$	NO$_3$	NH$_4$	EC	OC	Metals	Non-metals	Sulfate	NO$_2$	CO	SO$_2$	O$_3$
Correlation between various species, precursor gases and meteorological quantities (annual)												
$R_s\downarrow$	**−0.377**	**−0.488**	**−0.440**	**−0.497**	**−0.230**	−0.115	**−0.452**	**−0.479**	**−0.561**	−0.176	**−0.512**	**0.706**
v	**−0.165**	**−0.296**	**−0.280**	**−0.297**	**−0.220**	−0.102	**−0.286**	**−0.290**	−0.118	**0.066**	−0.233	**0.479**
dir	−0.010	−0.050	0.091	0.105	0.056	0.108	−0.057	0.090	**−0.173**	0.041	−0.132	0.042
v_{gusts}	**−0.017**	**−0.374**	**−0.341**	**−0.351**	**−0.241**	−0.119	**−0.341**	**−0.354**	**−0.328**	0.167	**−0.447**	0.578
T	**−0.294**	**−0.620**	**−0.648**	**−0.563**	**−0.284**	**−0.249**	**−0.684**	**−0.714**	**−0.716**	−0.122	**−0.771**	**0.591**
T_{max}	**−0.288**	**−0.598**	**−0.626**	**−0.548**	**−0.280**	**−0.231**	**−0.662**	**−0.692**	**−0.663**	−0.116	**−0.732**	**0.623**
T_{min}	**−0.278**	**−0.610**	**−0.637**	**−0.539**	**−0.268**	**−0.270**	**−0.668**	**−0.701**	**−0.739**	−0.131	**−0.780**	**0.496**
T_{fuel}	**−0.207**	**−0.599**	**−0.638**	**−0.581**	**−0.233**	**−0.185**	**−0.651**	**−0.696**	-.-	0.045	**−0.740**	-.-
$T_{fuel,max}$	**−0.201**	**−0.589**	**−0.613**	**−0.571**	**−0.242**	**−0.165**	**−0.627**	**−0.671**	-.-	0.029	**−0.709**	-.-
$T_{fuel,min}$	**−0.182**	**−0.568**	**−0.623**	**−0.546**	**−0.214**	**−0.219**	**−0.637**	**−0.680**	-.-	0.024	**−0.733**	-.-
RH	0.031	0.127	0.018	0.168	0.101	−0.135	0.025	0.022	−0.128	0.071	−0.060	−0.549
RH_{max}	−0.184	−0.412	−0.477	−0.335	−0.170	−0.234	−0.493	−0.524	−0.546	0.030	−0.590	0.140
RH_{min}	0.155	0.355	0.281	0.372	0.199	0.008	0.302	0.314	**0.166**	0.096	0.259	−0.696
Correlation between various species, precursor gases and meteorological quantities (cold season)												
$R_s\downarrow$	−0.311	**−0.130**	**−0.192**	**−0.148**	−0.264	−0.078	**−0.214**	**−0.198**	**−0.095**	−0.169	−0.168	**0.465**
v	−0.386	**−0.225**	**−0.221**	**−0.215**	**−0.292**	−0.105	**−0.220**	**−0.222**	−0.068	−0.063	−0.176	**0.495**
dir	0.059	**0.124**	**0.091**	**0.050**	**0.034**	**0.021**	**0.079**	**0.097**	**0.016**	0.080	−0.021	**−0.022**
v_{gusts}	−0.362	**−0.288**	**−0.287**	**−0.238**	**−0.338**	**−0.131**	**−0.277**	−0.291	**−0.112**	0.157	−0.282	0.514
T	−0.667	**−0.391**	**−0.562**	**−0.269**	**−0.504**	**−0.275**	**−0.603**	**−0.609**	**−0.487**	−0.128	**−0.621**	**0.427**
T_{max}	−0.631	**−0.347**	**−0.528**	**−0.242**	**−0.479**	**−0.267**	**−0.569**	**−0.575**	**−0.380**	−0.102	**−0.554**	**0.432**
T_{min}	−0.592	**−0.383**	**−0.520**	**−0.245**	**−0.456**	**−0.258**	**−0.554**	**−0.562**	**−0.533**	−0.125	**−0.625**	**0.358**
RH	−0.173	−0.073	−0.199	−0.003	−0.071	−0.107	−0.217	−0.222	**−0.437**	0.119	−0.336	−0.149
RH_{max}	−0.415	−0.254	−0.400	−0.134	−0.274	−0.192	−0.423	−0.446	**−0.455**	0.122	−0.469	0.121
RH_{min}	0.078	**0.069**	**0.019**	**0.102**	**0.117**	**0.008**	**0.019**	**0.020**	**−0.285**	0.090	−0.124	**−0.344**
Correlation between various species, precursor gases and meteorological quantities (warm season)												
$R_s\downarrow$	**−0.079**	**−0.079**	0.008	**−0.155**	**−0.115**	0.122	0.073	0.104	0.333	0.030	0.261	0.627
v	**−0.061**	**−0.041**	0.095	**−0.063**	**−0.086**	−0.053	0.091	0.151	0.101	0.335	−0.075	0.227
dir	0.007	**0.032**	**0.047**	0.013	−0.012	0.070	**0.046**	0.050	−0.130	0.015	−0.007	−0.040
v_{gusts}	**−0.070**	**−0.089**	**−0.022**	**−0.129**	**−0.098**	0.012	−0.007	0.030	0.061	0.311	−0.075	0.222
T	**0.116**	**0.025**	**−0.082**	0.029	0.046	0.034	−0.164	−0.212	0.003	−0.099	0.049	**0.058**
T_{max}	**0.105**	**0.026**	**−0.050**	0.063	0.016	0.080	−0.138	−0.131	0.255	−0.093	**0.173**	0.314
T_{min}	**0.104**	**0.020**	**−0.166**	−0.003	0.071	−0.130	−0.206	−0.345	−0.465	−0.139	−0.188	−0.483
T_{fuel}	0.079	**0.053**	**0.003**	0.006	0.028	0.081	−0.077	−0.059	-.-	−0.100	−0.646	-.-
$T_{fuel,max}$	**0.025**	**0.019**	**−0.008**	−0.029	−0.033	0.117	−0.054	0.004	-.-	−0.106	0.390	-.-
$T_{fuel,min}$	**0.109**	**0.047**	**−0.100**	0.048	0.046	−0.144	−0.200	−0.285	-.-	−0.101	−0.747	-.-
RH	0.062	**0.017**	**−0.148**	0.036	0.096	−0.191	−0.149	−0.259	−0.535	0.002	−0.217	−0.777
RH_{max}	0.015	−0.058	−0.160	−0.018	0.0154	−0.063	−0.128	−0.178	**−0.324**	0.021	**−0.082**	−0.438
RH_{min}	**0.057**	**0.0183**	**−0.108**	0.005	0.096	−0.202	−0.092	−0.210	−0.533	0.029	−0.266	−0.737